1-1-2012

Evaluating the Effect of Implementing Biologically Realistic Delays on Hepatitis C Kinetics and Associated Estimates of Antiviral Efficacy

Shabnam Shamloo
Ryerson University

EVALUATING THE EFFECT OF IMPLEMENTING BIOLOGICALLY REALISTIC DELAYS ON HEPATITIS C KINETICS AND ASSOCIATED ESTIMATES OF ANTIVIRAL EFFICACY

by

Shabnam Shamloo

B.Sc. Physics, Azad University, Tehran, Iran, 2007

A thesis

presented to Ryerson University

in partial fulfillment of the

requirements for the degree of

Master of Science

in the Program of

Biomedical Physics

Toronto, Ontario, Canada, 2012

Author's Declaration

I hereby declare that I am the sole author of this thesis. This is a true copy of the thesis, including any required final revisions, as accepted by my examiners.

I authorize Ryerson University to lend this thesis to other institutions or individuals for the purpose of scholarly research.

I further authorize Ryerson University to reproduce this thesis by photocopying or by other means, in total or in part, at the request of other institutions or individuals for the purpose of scholarly research.

I understand that my thesis may be made electronically available to the public for the purpose of scholarly research only.

Abstract

Evaluating the effect of implementing biologically realistic delays on hepatitis C kinetics and associated estimates of antiviral efficacy

Shabnam Shamloo

Master of Science, Biomedical Physics

Ryerson University, 2012

Mathematical modelling of hepatitis C virus (HCV) decay under antiviral therapy has allowed for the determination of antiviral efficacy and other important parameters. Current models of HCV infection are based on a set of ordinary differential equations (ODEs) and assume that infectious cell lifespans are exponentially distributed over time, meaning that every infected cell has an equal probability of dying at any time. Here, we introduce a new model which: (1) allows for a realistic eclipse phase delay between the moment of cell infection and the release of new virus; and (2) considers both exponential and gamma-distributed delays for the time spent by cells in the infectious state, continuously producing virus. To allow for the simplest mathematical form, we consider a multiple-stage ODE model which yields gamma-distributed delays. Application of this model to viral titer data for patients undergoing antiviral therapy leads to different conclusions when predicting parameter values.

Acknowledgements

I would like to express my deep and sincere gratitude to my supervisor, Dr. Catherine Beauchemin for guiding my research, for providing motivation, enthusiasm, and for her immense knowledge. Besides my supervisor, I would like to thank Dr. Benjamin Holder for his encouragement, his detailed and constructive comments and for his support throughout this research and the writing of this thesis. I would like to thank Dr. Hana Dobrovolny, for the insights she has shared. My sincere thanks also go to the members of my supervisory committee, Dr. Jordan Feld, Dr. Emily Heath and Dr. Michael Kolios, who provided helpful guidance during our meetings and Dr. Carl Kumaradas for accepting to be on my examining committee. The financial support of the Natural Sciences and Engineering Research Council (NSERC) and Ryerson University are gratefully acknowledged. Last but not least, I would like to thank my family.

To

My dear Milad

Table of Contents

List of Tables

List of Figures

Chapter 1

Introduction

Hepatitis is a general term meaning inflammation of the liver. The most common cause of hepatitis is viral infection, such as the hepatitis A, B, C, D and E viruses. Since viral hepatitis can develop with limited or no symptoms, a correct diagnosis can be made only by testing a patient's blood serum for the presence of specific viral antigens and/or antiviral antibodies [76]. Hepatitis C is the infectious disease caused by the hepatitis C virus (HCV), and results in severe inflammation of the liver. A small fraction of infected patients show spontaneous clearance of the HCV infection due to a successful immune response [41, 66], but the majority of infected patients become chronically infected and are at risk for developing serious liver disease [2, 66, 76]. About 150 million people are chronically infected with HCV worldwide [2,76]. HCV is the most common cause of liver cirrhosis, hepatocellular carcinoma and liver transplantation [2, 40, 76].

There is currently no vaccine for HCV, but it is curable in some patients using antivirals. HCV is an enveloped, single stranded positive strand RNA genome. There are 6 genotypes of HCV which each exhibit significant molecular and clinical differences, such as different responses to treatment [29,64,76]. Numerous drugs have been evaluated for HCV treatment, with interferon (IFN) combined with ribavirin (RBV) being, until recently, the most effective. Under these antivirals, a sustained virologic response (SVR),

i.e. undetectable levels of HCV RNA for at least 6 months after completion of HCV antiviral therapy, could only be achieved in $\sim 50\%$ of patients [68, 72]. As knowledge of the structure, function and life cycle of HCV has increased, new therapies have been developed, which target specific components of the HCV structure [71]. The addition of direct acting antivirals (DAAs) to the current standard therapy consisting of IFN + RBV has resulted in a significantly higher rate of SVR, approximately 70% [32, 44, 59].

A complete understanding of the viral life cycle and the host–virus–antiviral interactions has been impeded by the limitations of experimental studies (see, e.g., the review in [33]). The development of an in vitro model has been particularly difficult [8, 36, 54]. HCV replication highly depends on the cellular environment [8, 54, 70]. In recent years a permissive system has been developed to support the replication of HCV virus in vitro: the human hepatoma cell (Huh-7) sublines and the JFH-1 HCV strain [8, 70]. In spite of that, it is not clear how this very specific and restrictive cell-virus system (Huh-7 cells+ JFH-1 HCV virus) compares with a typical *in vivo* HCV infection [8]. Chimpanzees are a fairly adequate *in vivo* model for the disease [9, 70], but experimentally-infected chimpanzees develop milder HCV disease compared to humans [33, 70], and shorter HCV rate of clearance in these animals [19]. And the high monetary cost of research in chimpanzees has limited the availability of such data. Recently, small animal models have been used that are more available and less expensive, but they have a set of limitations [33, 70]. For example, mice models with human livers are immunodeficient and the host adaptive immune responses cannot be studied [7, 33].

Precisely characterizing HCV kinetics has been strongly limited by the absence of a reliable in vitro cell culture model for HCV. Thus, mathematical modelling of HCV RNA decay under antiviral treatment for infections in human patients has provided crucial insights into the virus kinetics under treatment. Current mathematical models have estimated parameters by analyzing HCV RNA decay in patients' blood serum under antiviral treatment. Analyses of HCV infection and treatment provide estimates of the

viral clearance rate, drug effectiveness and infectious cell lifespan [5, 15, 16, 18, 23, 26, 31, 49, 56, 61]. These models, however, rely on assumptions that are not biologically realistic and need reconsideration. For example, most models assume that, upon infection, a cell immediately starts to produce and release new virions, and that an infected cell might die immediately after infection or might live very long.

In Chapter 2, I will review current HCV kinetics models to summarize the successes and limitations of these models. In Chapter 3, I will present biological information on liver and viral replication dynamics which motivates the construction of a new model. In Chapter 4, a new viral infection model will be presented. In Chapter 5, models uninfected and infected steady states will be presented. In Chapter 6, I will analyze the new model and discuss the effect of the eclipse phase and alternatives for cell lifespan in the viral kinetic (VK) profiles and parameter estimations. In Chapter 7, I will fit both the original and new models to HCV RNA level of infected patients under treatment and compare the results. A summary of the overall work follows in Chapter 8.

Chapter 2

HCV mathematical models

Mathematical models of HCV kinetics have played an important role in studying HCV. Mathematical models have been used to explain the decay of virus in the blood under antiviral treatment, learn of the parameters driving virus-host dynamics in infected chimpanzees [19], analyze viral decline during liver transplantation [20], and model IFN-α inhibition of HCV kinetics in vitro [17]. The host-virus interactions which take place over the course of an HCV infection are summarized in Figure 2.1. These infection states and variables will be discussed at length in the remainder of this work.

Most HCV VK modelling efforts have been directed at explaining viral decay in patient blood under various antiviral treatment regimens [5,15,16,18,23,26,31,49,56,61]. Patients with chronic HCV have an approximately constant level of virus in the blood, but a short time after taking an antiviral, that level will decline in a characteristic way. The decline of virus in the blood, which is easily measured in frequent intervals by clinicians, reflects the state of the infection which is ongoing in the liver. Thus by studying the decline, we can understand the virus infection and the effectiveness of the particular treatment.

HCV VK modelling followed a number of breakthroughs in the understanding of the kinetics of the human immunodeficiency virus (HIV) by monitoring patient blood under

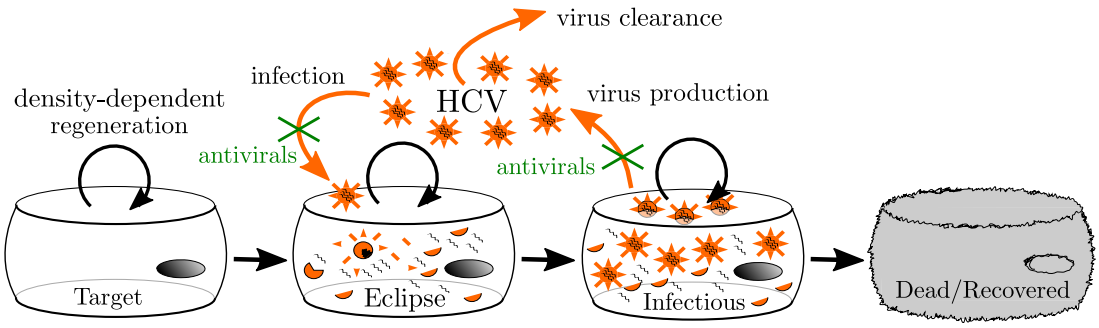

Figure 2.1: **Hepatitis C virus (HCV) infection progress model.** Target cells (T) are uninfected cells susceptible to infection by HCV. The interaction of virus with target cells leads to eclipse cells (E), newly infected cells which are not yet releasing virions as they must first synthesize viral proteins. Infectious cells (I) are cells that are actively producing virus for a period of time, before they transition into a state we will refer to as the dead or recovered state (D). These are cells which have ceased to produce virus either because they have undergone apoptosis or have spontaneously cured their intracellular infection but are not currently susceptible to infection. These cells are quickly replaced via regeneration of target, eclipse, and infectious cells. HCV (V) is produced by infectious cells at a constant rate and is lost over time due to systemic clearance. Antivirals act to either block viral production (e.g., interferon-α, some direct-acting antivirals) or affect viral infectivity (e.g., ribavirin, some direct-acting antivirals).

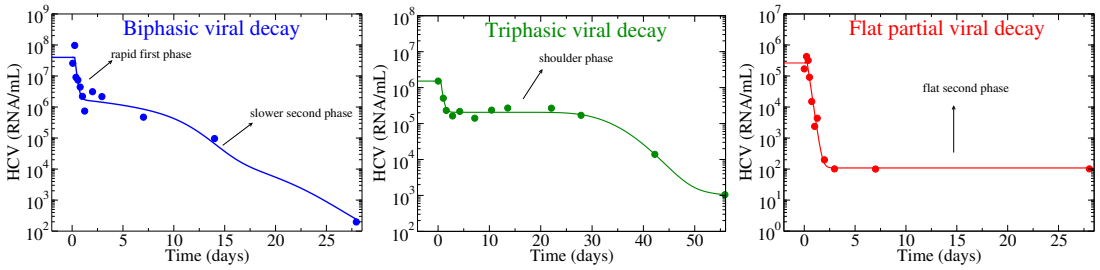

Figure 2.2: **Viral kinetic (VK) profiles under therapy.** A biphasic viral decay shows a rapid first phase drop in HCV RNA level in the few hours after initiation of treatment, followed by a slower second phase. In triphasic decay, the first rapid phase is followed by a shoulder phase, with no or little HCV RNA decline, and then a third phase of slow viral decay. In a flat partial decay, a rapid first phase decline is followed by a flat second phase, with little or no decline in HCV RNA level.

antiviral treatment [51, 55, 57, 58, 67]. Under antiviral therapy, it was observed that the level of HCV RNA in the blood of treated patients exhibits one of three distinct viral decay profiles: biphasic, triphasic and partial flat decays. An example of each is shown in Figure 2.2. The most common VK decline pattern is the biphasic decline [15,49], whereby a rapid first phase of decay is followed by a slower second phase. Triphasic and flat partial decays after antiviral therapy initiation have been observed in a smaller number of patients [5,31]. A triphasic decline consists of a rapid first phase, an intermediate flat shoulder phase, with no or very little viral decay, and a third, slower decay phase. In a flat partial decay, after a rapid first phase decline, the viral load steadies at a lower, non-zero value, resulting in a flat VK profile rather than a continued decay, hence "partial decay". A good model for HCV VK must be able to reproduce all of these VK decline patterns and yield biologically realistic parameter values.

2.1 The Neumann, Perelson, et al. model

The first mathematical model for HCV VK was introduced by Neumann et al. in 1998 [49]. It was based on the basic structure of the existing, and very successful, HIV VK

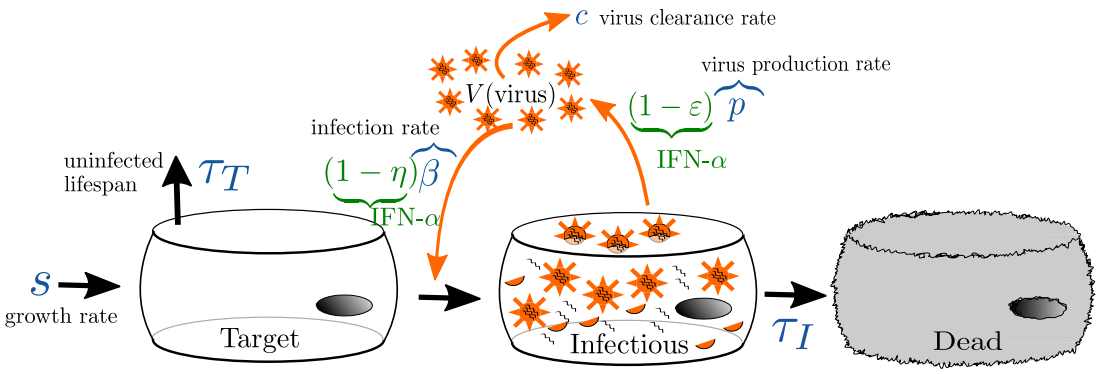

Figure 2.3: **Schematic representation of the Neumann, Perelson, et al. HCV model.** Target cells (T) are uninfected hepatocytes susceptible to infection by HCV (V) at infection rate β. Target cells grow at growth rate s and live for an average time τ_T. Infectious cells (I) are cells that are actively producing virus at a constant rate p with an average lifespan of τ_I. Free HCV in plasma is cleared at rate c. Antiviral therapy with IFN-α blocks virion production through parameter ε, while therapy with RBV reduces infection through parameter η.

model [51, 55, 58]. The Neumann et al. model is illustrated in Figure 2.3. This ordinary differential equations (ODE) model,

$$\begin{aligned}
\frac{\mathrm{d}T}{\mathrm{d}t} &= s - \frac{T}{\tau_T} - (1-\eta)\beta TV \\
\frac{\mathrm{d}I}{\mathrm{d}t} &= (1-\eta)\beta TV - \frac{I}{\tau_I} \\
\frac{\mathrm{d}V}{\mathrm{d}t} &= (1-\varepsilon)pI - cV \ ,
\end{aligned} \tag{2.1}$$

describes the interaction of target cells (T) with HCV virus (V) leading to infectious cells (I). Target cells are produced at growth rate s and die at rate $1/\tau_T$ (i.e., have an average lifespan of τ_T). Target cells are infected by HCV at infection rate β. Infectious cells actively produce virus and die (or stop producing virus) at rate $1/\tau_I$ (i.e., have an average infectious lifespan of τ_I). New virions are produced by infected cells at a constant rate p and cleared at constant rate c. The efficacy of IFN-α in blocking viral

production and the efficacy of RBV in reducing the infection rate are captured by ε and η, respectively. For example, IFN-α treatment efficacy in blocking 90% of virion production (i.e., reducing p by a multiplicative factor of 0.1) corresponds to $\varepsilon = 0.9$.

This model assumes that: (1) upon infection, a cell immediately starts to produce and release new virions; and (2) an infected cell might die immediately after infection or might live a very long time because the infectious cell lifespan is believed to follow an exponential distribution.

Since HCV is a chronic infection prior to initiation of therapy, the model is assumed to be in a steady state in the absence of treatment, i.e., $\frac{\mathrm{d}T}{\mathrm{d}t} = \frac{\mathrm{d}I}{\mathrm{d}t} = \frac{\mathrm{d}V}{\mathrm{d}t} = 0$. Setting the right hand side of model (2.1) equal to zero yields the steady state solution ($\bar{T}, \bar{I}$ and $\bar{V}$) in terms of the parameter values.

In order to fit patient data and estimate important parameters the modellers divide the time into two phases over which different simplifying assumptions are made. The first two days after initiation of drug, and treatment duration longer than two days. On the first 2 days, the infected cells do not die and the target cells are initially at steady-state, $T(t) = \bar{T}$ and $I(t) = \bar{I}$. In making this assumption, model (2.1) is reduced to a single equation which depends on c and ε. Using this equation to fit the first two days of VK decline post-treatment makes it possible to determine these parameters. The fitting results against patient data showed that the first phase decline starts after a waiting time ~ 9 h [49], which is believed to reflect drug pharmacokinetics/pharmacodynamics and lasts about ~ 2 days [49]. HCV RNA level decays by 1 to 2 logs during that time. It was concluded that the major mechanism of IFN action is to block virus production by reducing it such that $p \to (1 - \varepsilon)p$, with the first phase of viral decline dependent only on drug efficacy, ε, and the viral clearance rate, c.

Over longer periods, the infectious cells death cannot be ignored. But target cells are assumed to be constant during the longer time, which allows for the analytical solution of Eqs. (2.1). Infectious cell lifespan τ_I can then be estimated by substituting in obtained

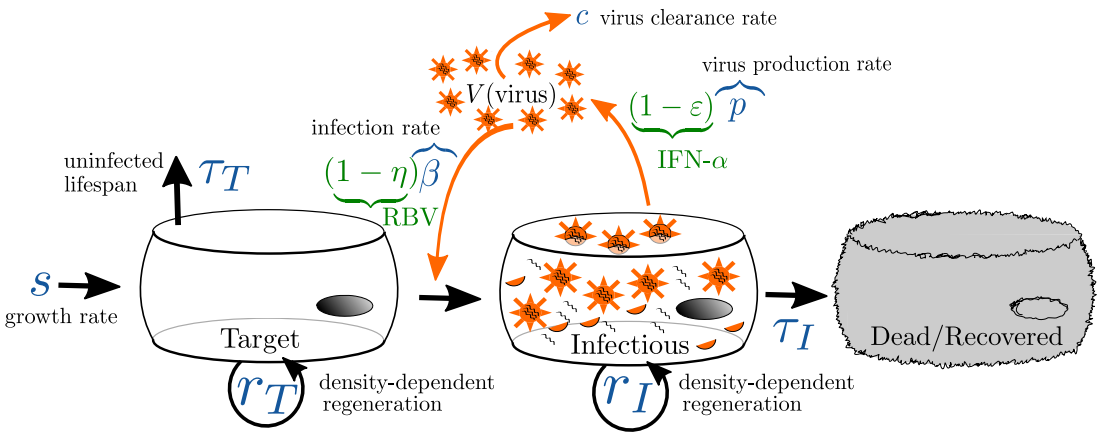

Figure 2.4: **Schematic representation of the NDP HCV model.** Target cells (T) are uninfected hepatocytes susceptible to infection by HCV (V). Target cells interaction with HCV leads to productively infectious cells. Target cells and infectious cells regenerate at rate r_T and r_I, respectively. Target cells grow at growth rate s and die after time τ_T passes. Infectious cells actively produce virions at a constant rate p per unit time. After time τ_I passes infectious cells stop producing new virus. Hepatitis C virions are cleared at rate c. Initiation of antiviral can either dampen viral production to $(1-\varepsilon)p$ or reduce viral infectivity β to $(1-\eta)\beta$.

values for ε and c into the analytical solution, and fitting it against 14 days data [49].

The typical response to antiviral treatment is a biphasic viral decline which this model could reproduce. However, a number of patients exhibit triphasic viral decline under antiviral therapy [31] which an accurate model should be able to reproduce. Unfortunately, the Neumann, Perelson, et al. model is not able to capture the triphasic virus decline.

2.2 The NDP model

Dahari et al. (2007) [18] extended the Neumann, Perelson, et al. model by including proliferation of both uninfected and infected hepatocytes. We will refer to this extended model as the NDP model in the remainder of this document. The extended, NDP model, is illustrated in Figure 2.4. Mathematically, the NDP model,

$$\begin{aligned}
\frac{\mathrm{d}T}{\mathrm{d}t} &= s + r_T T\left(1 - \frac{T+I}{T_{\max}}\right) - \frac{T}{\tau_T} - (1-\eta)\beta TV \\
\frac{\mathrm{d}I}{\mathrm{d}t} &= r_I I\left(1 - \frac{T+I}{T_{\max}}\right) + (1-\eta)\beta TV - \frac{I}{\tau_I} \\
\frac{\mathrm{d}V}{\mathrm{d}t} &= (1-\varepsilon)pI - cV \ ,
\end{aligned} \tag{2.2}$$

contains much of the same terms and parameters described above in Section 2.1. In addition, it includes the density-dependent proliferation of uninfected and infected hepatocytes at rates r_T and r_I, respectively, following logistic growth constrained by the maximum number of susceptible hepatocytes $T_{\max}$.

Including regeneration of both infected and uninfected cells enables this model to reproduce triphasic viral kinetics [22]. The model predicts that a triphasic decline occurs only in patients where almost all susceptible hepatocytes are chronically infected with HCV ($I \gg T$), i.e., when the population of target cells is 2 to 4 orders of magnitude smaller than the number of infectious cells. This VK is illustrated in Figure 2.5. During the shoulder (intermediate) phase, the infectious cell population is almost constant due to infected cell regeneration. The HCV RNA level, which is in quasi-steady state with the productively infectious cells, is also approximately constant. Meanwhile, target cells regenerate and target cell numbers increase until they approach the infectious cells level. At this point regeneration of infectious cells will be forced to reduce due to the density-dependent form of regeneration term. Thus, the infectious cell population starts declining, followed by the virus decay, and the shoulder phase ends. A larger growth rate of uninfected hepatocytes, s, can shorten the length of shoulder phase [18].

Also the extended model by Dahari et al. explains the viral kinetics seen in flat partial responders without imposing long infectious cell lifespan [31]. The model predicts that when the ratio of uninfected to infected cells is very high and generation of uninfected cells is not much higher than that of infected cells the shoulder phase does not stop and leads to partial flat decay profile [22]. The model shows that the last phase of viral decay

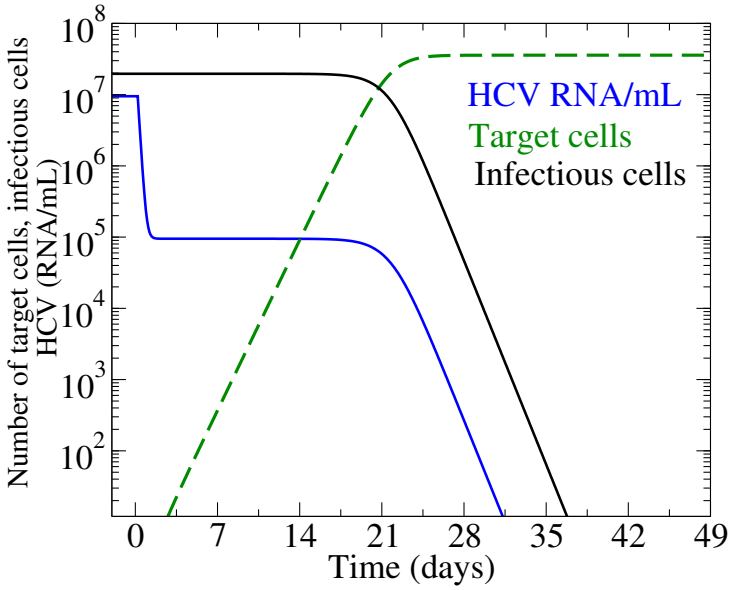

Figure 2.5: **Triphasic viral decline in the NDP model.** In the first two days HCV RNA decay depends on the viral clearance rate and the antiviral efficacy, therefore we can see a rapid drop in the HCV RNA level (blue line). In a shoulder phase, there is a very little decrease in HCV RNA. During this phase infectious cell population (Black line) is almost constant due to infected cells regeneration. Therefore HCV RNA level, which is in quasi-steady state with the productively infectious cells, is approximately constant. Meanwhile target cells (green dashed-line) regenerate until approach the infectious cells level. At this point regeneration of infectious cells will be forced to reduce due to the density-dependent form of regeneration term. Infectious cells hence virions start declining and shoulder phase ends.

is determined by the infected cells lifespan (loss rate of infected cells) and the antiviral efficacy [22].

The extended model by Dahari successfully reproduces the different HCV kinetics — biphasic, triphasic and flat partial decline — seen in patient data [18].

2.3 Does the NDP model yield realistic parameters?

Over the past decade, the NDP model has been very helpful in understanding HCV VK under treatment and estimating key infection parameters. This model provides a good fit to the patient data. For example, a fit of the NDP model to patient data from Reluga et al. [61] is shown in Figure 2.6. This fit yielded estimates of $c = 5.40$ day^{-1} for the viral clearance rate, $\tau_I = 7.69$ days for infectious cells lifespan and IFN efficacy of $\varepsilon = 0.996$. However, in this particular fit, the parameters imply that this chronically infected liver is only about 58% of its original size, and 96% of the hepatocytes that make up this shrunk liver are infected. Are these numbers biologically realistic?

Literature reports suggest that the livers of HCV-infected patients are not observed to shrink, i.e. it is unlikely that chronically HCV-infected livers are less than 90% of their uninfected size. Reports of the fraction of the fraction of the liver chronically infected with HCV vary with some reporting 1% to 81% of the liver infected [1, 24, 65] and other suggesting that 100% of the liver is actually infected [52]. So certainly, HCV-infected livers should be no smaller than about 90% of their uninfected size, and $\geq 1\%$ of liver cells should be infected by HCV.

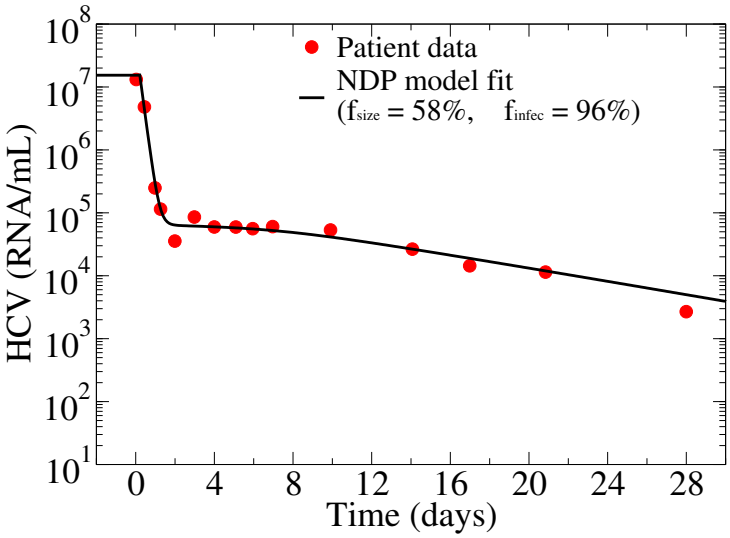

Figure 2.6: **Fit of the NDP model to HCV RNA levels under peg-IFN-α-2a therapy.** The fit is from Reluga et al. 2009 [61], but the original patient data is from Hermann et al. [31]. Parameter values are $c = 5.4\ \mathrm{d}^{-1}$, $\tau_I = 7.69\ \mathrm{d}$, $r_T = 1.1\ \mathrm{d}^{-1}$, $r_I = 0.26\ \mathrm{d}^{-1}$, $s = 1\ \mathrm{cells} \cdot \mathrm{mL}^{-1} \cdot \mathrm{d}^{-1}$, $\tau_T = 83\ \mathrm{d}$, $p = 13.2\ \mathrm{virus} \cdot \mathrm{cell}^{-1} \cdot \mathrm{d}^{-1}$, $\beta = 2.8 \times 10^{-8}\ \mathrm{mL} \cdot \mathrm{virus}^{-1} \cdot \mathrm{d}^{-1}$, $T_{\max} = 1.2 \times 10^7\ \mathrm{cells} \cdot \mathrm{mL}^{-1}$ and $\eta = 0$, $\varepsilon = 0.996$. Parameters are such that the infected liver is 58% of its original size and is 96% infected.

Chapter 3

HCV biology to inform the construction of mathematical models

Building a detailed mathematical model of HCV infection requires close consideration of the biological processes. In this chapter, we look at biological details which inform the mathematical specifics and in some cases the parameter value selection for this model. This chapter provides evidence that an eclipse phase should be used and that cell death of a variety of types should be considered. We will consider details of the NDP model (e.g., regeneration, delays between infection phases) and make additions/revisions based on biological evidence. We describe the precise implementation of these ideas when we introduce the γ-model in Chapter 4.

3.1 Delays between phases of infection

HCV infections in vitro have shown that following the infection of cells, there is a delay prior to the production of virus [30, 36, 79]. In vitro experiments report the disappear-

ance of input virus from the cell culture medium (supernatant) for a short time after infection and before the start of significant virus production [30, 36, 79]. This temporary disappearance of the inoculation virus suggests that there is a pause between the entry of the virus into cells (infection) and the start of virus production in these newly infected cells. This pause, known as the eclipse phase occurs because translation and replication of the key viral proteins must first take place before viral assembly and release can occur [4,21,37]. After a few hours, however, virus can be detected again [30,36], indicating that newly infected cells are progressively starting to come out of the eclipse phase and are beginning to produce virus. Also it has been suggested that HCV infection might induce an antiviral defense pathway within infected cells which could be responsible for delaying viral replication and detection of infectious virus for days [79]. Therefore to have a more biologically–realistic model, a delay between cell infection and release of a new virions should be implemented. We build an eclipse phase into the model to account for known delays between the infection of a cell and virus release. The eclipse phase should be such that it imposes a minimum waiting period between cell infection and virus production such that newly infected cells cannot begin producing virus immediately upon infection.

Once cells in the eclipse phase begin virus production, i.e. become infectious cells, they will produce virus for a time but will eventually cease viral production. There are a number of processes by which an infectious, virus-producing, hepatocyte may cease to produce virus, and each requires a specific mathematical implementation to ensure the process is accurately captured. We consider four different processes (Figure 3.1).

First, HCV infection induces cells apoptosis in the liver of HCV infected patients [3, 10, 25]. It is widely accepted that apoptosis of virus-infected cells happens to protect host cells against viral infection. One possibility is that the infected cell might die due to the accumulation of viral proteins in the host cell [3, 25, 34] caused by virion production. Analysis of HCV virus-infected cells on the hepatocyte cell cycle in vitro revealed that cells replicating HCV RNA exhibited increased apoptosis by accumulation of core and

nonstructural proteins of HCV [13, 35, 69]. In this process, a newly infected cell is not at risk of undergoing apoptosis because it contains very few viral proteins. However, after a cell has been infected for some time, it will have accumulated a certain number of viral proteins, and once that number reaches some critical threshold the cell will cease viral production and undergo apoptosis. This process therefore requires a certain waiting period wherein newly infected cells would not cease viral production.

Another possibility *in vivo* is that infected cells die due to host immune response attack [3, 11, 25, 34]. Because HCV causes chronic infection, the immune response is present at all times. The probability of immune response induced cell death is constant in time. It is important to emphasize that one of these processes occurs following a sequence of events (e.g., the buildup of viral toxicity) while the other may occur at any moment of time with equal probability.

Rather than dying, it is possible an infectious cell would cease viral production because it spontaneously cures the infection within it. This has been observed in HCV replication in vitro with a high frequency of cured cells in the presence of IFN-α [8]. Cell cure can happen through the activation of a pathway triggered as part of viral replication [8,11]. Much like cell death, the process of cell cure may occur spontaneously with equal probability at any time interval, e.g., due to the continuous presence of an extracellular curing agent, or as a result of some timed sequence of events. e.g., if the cycle of viral replication activates an intracellular antiviral pathway capable of clearing intracellular HCV.

The implementation of different timings for the transitions between stages of infection in a mathematical model are accomplished by "delay distributions" which specify the statistics of a particular transition time. One way to look at the delay distributions is shown in Figure 3.2, where the probability that a cell has *not* transitioned is shown as a function of time. A biological process which is in some sense "timed", i.e., occurring after a sequence of events after some time has elapsed can be represented by a gamma

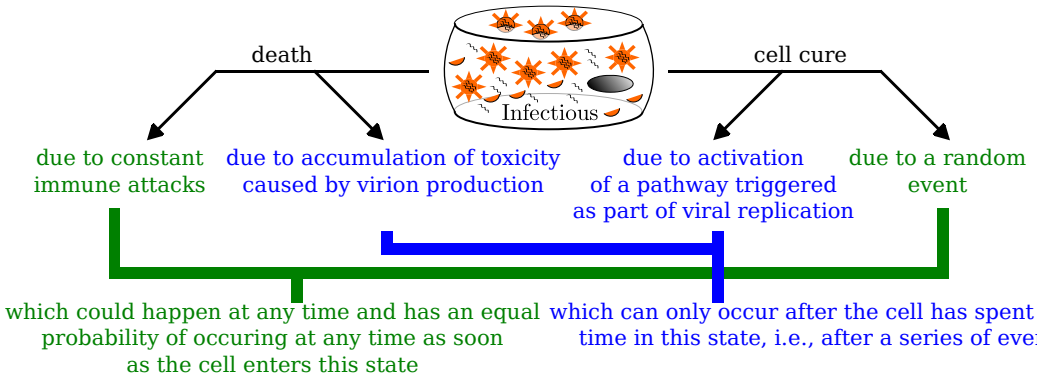

Figure 3.1: **Four different processes which lead to infectious cells loss.**

distribution. A process which can occur with equal probability in any interval of time is given by the exponential distribution (for which the hazard rate is constant) [53].

Based on the discussion above, the transition from the eclipse to infectious state is best represented by a gamma distribution, rather than an exponential distribution because the former provides a fixed period over which the probability of transitioning is essentially zero. The transition out of the infectious phase, however, could be described by either the exponential or gamma distribution, depending on the dominant process responsible for the cessation of viral production by infectious cells.

As we will describe in Chapter 4, the gamma-distributed multi-stage ordinary differential equation model allows for the implementation of either of these types of transitions.

3.2 Cell regeneration

Studies of liver regeneration and repair has shown a high regeneration capacity of liver in human and animals [12,27,47,75,77]. Hepatocytes are generally in a non-proliferative state, but in the case of liver injury they leave their quiescence (G_0) state and undergo replication [12, 27]. There is evidence of stem cells present in livers with the ability to differential into, and regenerate hepatocytes. But, hepatocytes replacement by stem cells is a rare event [27,75], and such cells are not always detectable [27]. Therefore, it is

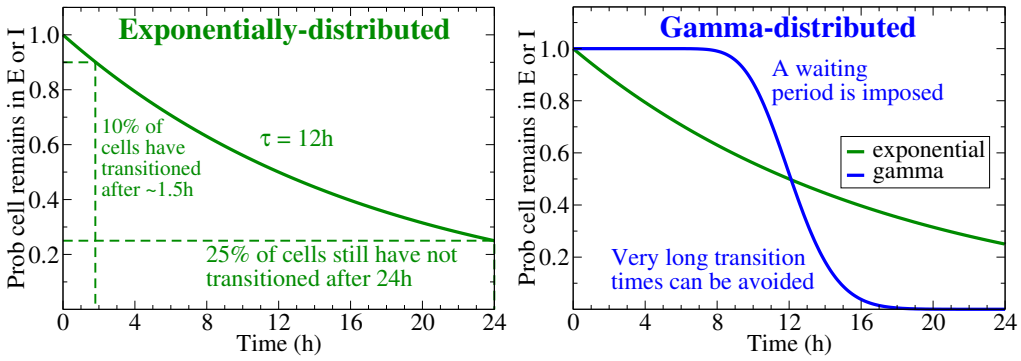

Figure 3.2: **Representations of different delay distributions defining the random time spent by a cell in its current state before transitioning to the next.** For each distribution type, a function is shown representing the probability that a cell remains in a given state (where the median time is 12 h). An exponential distribution for the lifespan of an infected cell allows for immediate transition to next state (e.g., 10% of cells have transitioned after $\sim$ 1.5 h has passed) and allows long transition times (e.g., 25% of cells still have not transitioned after 24 h). A gamma distribution enforces a minimum waiting period before cells can transition to the next state and allows most of the cells transition to next state within a narrow range of time about the median time, 12 h, thus avoiding very long transition times.

believed the main source of liver regeneration after injury is from existing hepatocytes and does not require activation of stem cells [27, 46, 75].

Studies of human liver regeneration after liver transplantation demonstrate rapid hepatocytes regeneration after hepatectomy. The analysis of liver regeneration indicates that normal livers regenerate at least twice as fast as infected livers [47, 77], perhaps because of infected cells' apoptosis [34]. In vitro studies of HCV infection and cellular proliferation reported that HCV infection slows down the hepatocyte regeneration rate [34, 73]. Timpe et al. [73] observed doubling times of 32 h and 34 h for uninfected and infected cells, respectively. There is a small difference between the two observed regeneration times, but it is not statistically significant unlike the important difference observed in liver transplantation studies. This might be due to absence of interferon in vitro, whereas their presence *in vivo* might further reduce the regeneration rate in HCV-infected livers [17].

In order to determine the uninfected and infected hepatocyte regeneration rate as precisely as possible, we attempted to use all available data to fit observed regeneration to a realistic, logistic growth model. To estimate hepatocytes regeneration rate, liver volume data from liver resection experiments were fitted [47, 77]. Liver volume were monitored with computed tomography after major hepatic resection in adult patients [47,77]. In these experiments, liver volume is expressed as a percentage of the volume of the liver prior to resection. To fit this data we used a density dependent cell regeneration process [19] which describes the balance between hepatocyte regeneration and apoptosis [12]. Uninfected and infected hepatocytes can regenerate at maximum regeneration rates r_T and r_I, respectively, under the control of a homeostatic process in which proliferation shuts down as the total number of hepatocytes approaches a maximum number $T_{\max}$ [19]. Density-dependent regeneration is modelled as

$$\frac{\mathrm{d}H}{\mathrm{d}t} = rH\left(1 - \frac{H}{N}\right)$$

where H is the percent liver volume (%) i.e. its volume relative to that prior to resection, r the hepatocytes regeneration rate, N the maximum liver volume size. This expression leads to exponential growth at a rate that is density-dependent since the regeneration rate is proportional to $(1 - \frac{H}{N})$, such that it is largest when $\frac{H}{N}$ is smallest (i.e. when $H \ll N$). The analytical solution to this equation is:

$$H(t) = \frac{N}{1 + (\frac{N}{H_0} - 1)\ \mathrm{e}^{-rt}} \tag{3.1}$$

where H_0 is the liver volume at time $t = 0$ after liver resection, expressed as the percent of liver remaining relative to its volume before resection.

Eq. (3.1) is fitted to liver resection data from several patients (Figure 3.3) and estimated both infected and uninfected hepatocytes regeneration rates. It is assumed that in a normal liver all hepatocytes are uninfected, and that in HCV-infected livers all

hepatocytes are infected, for simplicity. The average regeneration rates from these fits were found to be $r_T = 0.12$ d^{-1} in normal livers, and $r_I = 0.05$ d^{-1} in chronically HCV-infected livers. It is clear from the fits in Figure 3.3, that the logistic model appropriate captures the observed growth. In particular, the addition of a term to account for potential *de novo* growth from stem cells, namely the s term which appears in the NDP model (2.2), does not seem to be warranted by the data.

3.3 Liver size and fraction of the liver chronically infected

Biological information about chronically HCV-infected liver helps us to constraint our mathematical model in a more realistic biologic manner and leads to more realistic parameter value prediction for the model:

The target cells for HCV are liver hepatocytes. Hepatocytes are estimated to number approximately 10^{11} cells in the liver of normal adult human with a standard weight of 70 kg [45].

The fraction of hepatocytes that are infected in chronically infected patients is not well known. Agnello et al. (1998) [1] reported fraction of liver infected range 15–81% in different patient biopsy HCV RNA detection, while Lucas et al. (2001) [24] reported 1–71%, Vona et al. (2004) [74] reported 1–40%, Rodriguez-Inigo et al. (2005) [65] reported 4.9–7.1% and recently Nuriya et al. (2010) [52] reported that almost all hepatocytes are infected with HCV in chronic liver disease. This wide range of liver infection might be due to biopsy size, which can strongly influence the fraction of liver infected estimation [14]. However the fraction of liver chronically infected play an important role in VK results, so the model will be written in terms of fraction of liver infection and explore both ends of spectrum.

The change in liver size due to chronic hepatitis infection is unknown, but is probably not large, i.e. it is unlikely that chronically HCV-infected livers shrink more than 10% of their uninfected size. The infected liver size compare to original uninfected liver size play

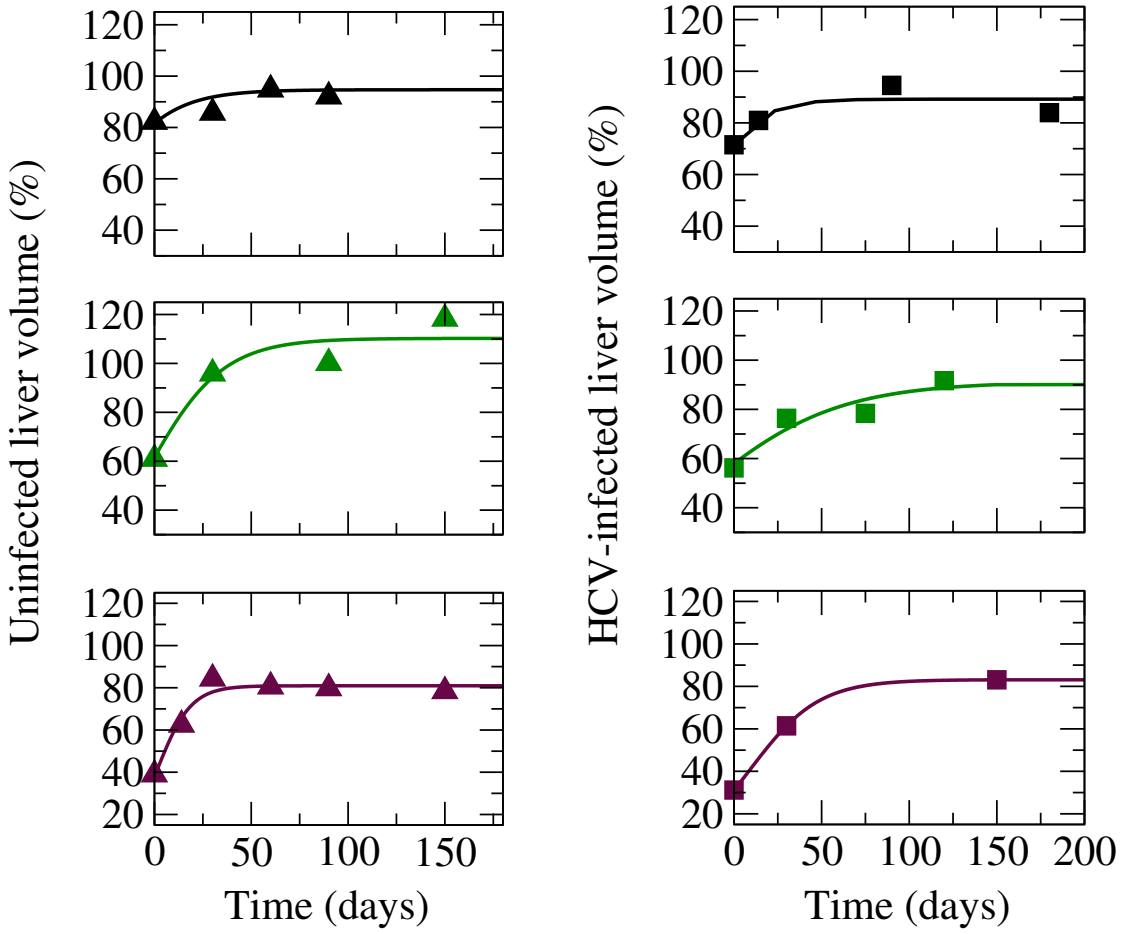

Figure 3.3: **Fits of the logistic cell regeneration model to liver resection data from patients.** Each graph presents a liver volume change in a patient who underwent small-range (black line), middle-range (green line) and large-range resection (maroon line). Patients were either uninfected (left) or chronically infected with HCV (right). Normal liver and chronic hepatitis liver volume data from Yamanaka et al. 1993 [77]. Fit of Eq. (3.1) to experimental data estimated the average regeneration rate of $r_T = 0.12$ d^{-1} and $r_I = 0.05$ d^{-1} in normal and chronic hepatitis liver, respectively.

an important role in defining and estimating the fraction of liver infected. In Chapter 5, we will describe it mathematically and use it as a biological constraint on our model. Further in Chapter 7, while fitting mathematical models against patient data, we will explore its effect on evaluating fraction of liver infected.

Chapter 4

A new γ-model for HCV infections

In this chapter, we construct a model for HCV infection and its treatment with antivirals which, while remaining simple in structure, is faithful to the known biology of the human liver and HCV VK. In Chapter 2, we presented the current state of HCV modelling, and emphasized that these models implicitly (1) neglect any delay between infection and viral production, and (2) assume that the timing of cell death is exponentially-distributed. However, in Chapter 3, we presented evidence from the literature that viral production immediately after infection is not possible, and that a more realistic model of the transition to virus production would require an eclipse delay prior to virus production. In Chapter 3, we also discussed a variety of reasonable processes by which infected cells could die, or cease viral production, some of which imply the time spent by a cell in the infectious phase is best represented by an exponential distribution, while others require that a delay, such as that provided by a gamma-distribution, be enforced.

Thus, we construct a model which allows for more general assumptions about the eclipse phase prior to viral production and the manner in which infectious cells die, and which includes realistic estimates of biological quantities to constrain parameter values

and restrict HCV kinetics.

4.1 A gamma-distributed model of HCV infection

One way of implementing more realistic delay distributions into the model is the method of stages [38,39], in which the phase which requires a delay is divided into n exponentially-distributed stages, such that a certain phase (e.g., eclipse, infectious) is the sum of n exponential stages.

The new γ-model with a gamma-distributed eclipse phase and a gamma-distributed infectious cell lifespan is given by

$$\begin{aligned}
\frac{\mathrm{d}T}{\mathrm{d}t} &= -(1-\eta)\beta TV + r_T T\left(1-\frac{T+E+I}{T_{\max}}\right)\\
\frac{\mathrm{d}E_1}{\mathrm{d}t} &= (1-\eta)\beta TV - \frac{n_E}{\tau_E}E_1 + r_E E_1\left(1-\frac{T+E+I}{T_{\max}}\right)\\
\frac{\mathrm{d}E_i}{\mathrm{d}t} &= \frac{n_E}{\tau_E}(E_{i-1}-E_i) + r_E E_i\left(1-\frac{T+E+I}{T_{\max}}\right) \qquad \text{for } i=2,3,...,n_E\\
\frac{\mathrm{d}E_{n_E}}{\mathrm{d}t} &= \frac{n_E}{\tau_E}(E_{n_E-1}-E_{n_E}) + r_E E_{n_E}\left(1-\frac{T+E+I}{T_{\max}}\right)\\
\frac{\mathrm{d}I_1}{\mathrm{d}t} &= \frac{n_E}{\tau_E}E_{n_E} - \frac{n_I}{\tau_I}I_1 + r_I I_1\left(1-\frac{T+E+I}{T_{\max}}\right)\\
\frac{\mathrm{d}I_i}{\mathrm{d}t} &= \frac{n_I}{\tau_I}(I_{i-1}-I_i) + r_I I_i\left(1-\frac{T+E+I}{T_{\max}}\right) \qquad \text{for } i=2,3,...,n_I\\
\frac{\mathrm{d}I_{n_I}}{\mathrm{d}t} &= \frac{n_I}{\tau_I}(I_{n_I-1}-I_{n_I}) + r_I I_{n_I}\left(1-\frac{T+E+I}{T_{\max}}\right)\\
\frac{\mathrm{d}V}{\mathrm{d}t} &= (1-\varepsilon)pI - cV
\end{aligned} \tag{4.1}$$

where $E=\sum_{i=1}^{n_E}E_i$ and $I=\sum_{i=1}^{n_I}I_i$, such that

$$\begin{aligned}
\frac{\mathrm{d}E}{\mathrm{d}t} &= (1-\eta)\beta TV - \frac{n_E}{\tau_E}E_{n_E} + r_E E\left(1-\frac{T+E+I}{T_{\max}}\right)\\
\frac{\mathrm{d}I}{\mathrm{d}t} &= \frac{n_E}{\tau_E}E_{n_E} - \frac{n_I}{\tau_I}I_{n_I} + r_I I\left(1-\frac{T+E+I}{T_{\max}}\right).
\end{aligned}$$

Most terms in this model are from the NDP model, and are as described in Sections 2.1 and 2.2. The new terms and parameters of this model have to do with the addition of an explicit eclipse phase, E, corresponding to newly infected cells not yet producing virus. The model formulation also enables the implementation of realistic delays for the eclipse and infectious phases. The new parameters are as follows. Parameters n_E and n_I are the number of eclipse and infectious stages, yielding gamma-distributed duration for the eclipse and infectious phases, of mean durations τ_E and τ_I, and standard deviations, $\tau_E/\sqrt{n_E}$ and $\tau_I/\sqrt{n_I}$, respectively. This makes n_E and n_I the gamma-distribution shape parameters, and τ_E/n_E and τ_I/n_I the scale parameters, i.e. the inverse of the rate parameters.

Note that this model allows us to model both exponential distributions for the time spent by cells in the eclipse or infectious phase (by setting n_E and/or n_I to 1), or to impose a minimum waiting period (by setting n_E and/or n_I to be larger than 1). In the remainder of this document, when we make mention of gamma-distributed delays, we imply that n_E and/or $n_I > 1$, such that a minimum waiting time is imposed before cells can transition to the next state.

Chapter 5

Steady states to represent chronic HCV infections

During chronic infection, before initiation of antiviral therapy, the level of serum HCV RNA does not vary significantly over time [50]. Since treatment is administered when a patient suffers from chronic infection, HCV VK under antiviral therapy is simulated by first setting the model to an infected steady state before applying treatment. The steady state in any model is achieved by setting $\frac{\mathrm{d}T}{\mathrm{d}t} = \frac{\mathrm{d}E}{\mathrm{d}t} = \frac{\mathrm{d}I}{\mathrm{d}t} = \frac{\mathrm{d}V}{\mathrm{d}t} = 0$, which yields the steady state solution ($\bar{T}, \bar{E}, \bar{I}$ and $\bar{V}$) in terms of the parameters of the model. Note that another, uninfected steady state, exists in each model and can be found by additionally requiring that $\bar{E} = \bar{I} = \bar{V} = 0$, yielding $\bar{T}_{\mathrm{uninf}}$, the number of hepatocytes in an uninfected liver.

The NDP and γ HCV models are used to fit patient data whose functional form is relatively simple (biphasic, triphasic, or flat). Such simple VK only allows for the determination of a small number of parameters. The NDP model has a total of 9 parameters (r_T, r_I, s, τ_T, τ_I, β, p, c, and $T_{\max}$), and the γ-model has 11 parameters (r_T, r_E, r_I, τ_E, τ_I, n_E, n_I, β, p, c and $T_{\max}$). In addition, under antiviral therapy, both the NDP and γ-model have up to two additional parameters for the antiviral efficacy of IFN (ε) and

RBV (η). Therefore, reducing the number of free parameters in each model is important.

The steady state values of the variables ($\bar{T}$,$\bar{E}$,$\bar{I}$,$\bar{V}$) are all set by the equilibrium equations if all parameters are known. The steady state equations, together with biologically realistic estimates of liver and HCV parameters, can be used to constrain model parameters and steady state variables. But this requires that parameters be known, measurable, or relatable to experimentally measurable quantities.

The value of the infectious cell lifespan in vivo (τ_I), the viral production rate (p), and the rate of cell infection by HCV (β), are poorly known and cannot easily be obtained experimentally. Therefore, we decided to introduce three additional, more biologically relevant, parameters:

$\bar{T}_{\mathbf{uninf}}$ the number of hepatocytes in the uninfected liver;

$f_{\mathbf{size}}$ the steady state size of the chronically HCV-infected liver expressed as a fraction of its size when uninfected; and

$f_{\mathbf{infec}}$ the fraction of hepatocytes of the chronically HCV-infected liver which are infected (i.e., either in the eclipse or infectious state).

The latter two quantities can be expressed mathematically for both models as

$$f_{\text{size}} = \frac{\bar{T} + \bar{E} + \bar{I}}{\bar{T}_{\text{uninf}}}$$
$$f_{\text{infec}} = \frac{\bar{E} + \bar{I}}{\bar{T} + \bar{E} + \bar{I}} \, .$$

In the remainder of this work, we will consider $\bar{T}_{\text{uninf}}$, f_{size}, and f_{infec} for their biological realism, and will use them to replace τ_I, p, and β which instead will be expressed as a function of, and computed using, the former three quantities.

5.1 Steady states in the NDP model

We can find the total number of hepatocytes in the uninfected liver, $\bar{T}_{\text{uninf}}$, from the uninfected steady state by setting the equations of model (2.2) equal to zero and imposing $\bar{V} = \bar{I} = 0$, such that the total number of hepatocytes in the uninfected liver is given by:

$$\bar{T}_{\text{uninf}} = \frac{T_{\max}}{2r_T}\left[r_T - \frac{1}{\tau_T} + \sqrt{\left(r_T - \frac{1}{\tau_T}\right)^2 + \frac{4r_T s}{T_{\max}}}\right] .$$

The infected steady state is achieved by setting the equations of model (2.2) equal to zero, such that

$$\begin{aligned}
\bar{V} &= \frac{r_T(1-f_{\text{size}})}{\beta} - \frac{1}{\beta\tau_I} + \frac{sp\tau_I}{r_I c\tau_I(1-f_{\text{size}}) - c} \\
\bar{T} &= \frac{c}{\beta p\tau_I} - \frac{r_I c(1-f_{\text{size}})}{\beta p} \\
\bar{I} &= \frac{c\bar{V}}{p},
\end{aligned}$$

As explained above, by introducing $\bar{T}_{\text{uninf}}$, f_{size}, and f_{infec}, we can replace the more poorly known parameters τ_I, p, and β by expressing them as a function of these former three quantities and other model parameters, such that they can simply be computed as

$$\tau_I = \frac{\bar{T}_{\text{uninf}} f_{\text{infec}} f_{\text{size}}}{s} - \frac{\tau_T f_{\text{infec}}}{(1-f_{\text{infec}})} + \frac{f_{\text{infec}}}{r_T(1-f_{\text{infec}})r_I f_{\text{infec}}}\left(\frac{T_{\max}}{T_{\max} - \bar{T}_{\text{uninf}} f_{\text{size}}}\right) \tag{5.1}$$

$$p = \frac{c\bar{V}}{f_{\text{size}} f_{\text{infec}} \bar{T}_{\text{uninf}}} \tag{5.2}$$

$$\beta = \frac{f_{\text{infec}}}{\bar{V}\tau_I(1-f_{\text{infec}})} - \frac{r_I f_{\text{infec}}}{\bar{V}(1-f_{\text{infec}})}\left(1 - \frac{\bar{T}_{\text{uninf}} f_{\text{size}}}{T_{\max}}\right) \tag{5.3}$$

5.2 Steady states in the γ-model

Like for the NDP model, the total number of hepatocytes in the uninfected liver, $\bar{T}_{\text{uninf}}$, can be found from the uninfected steady state of the γ-model by imposing $\bar{V} = \bar{E} = \bar{I} =$

0, such that

$$\bar{T}_{\text{uninf}} = T_{\max} \ .$$

The infected steady state of γ-model is achieved by setting the equations of model (4.1) equal to zero, yields the infected steady state solutions

$$\begin{aligned}
f_{\text{infec}} = \frac{\bar{E}+\bar{I}}{\bar{T}+\bar{E}+\bar{I}} \quad &\rightarrow \quad \bar{E}+\bar{I} = T_{\max} f_{\text{size}} f_{\text{infec}} \\
f_{\text{size}} = \frac{\bar{T}+\bar{E}+\bar{I}}{T_{\max}} \quad &\rightarrow \quad \bar{T} = T_{\max} f_{\text{size}}(1-f_{\text{infec}}) \\
\beta\bar{V} = r_T(1-f_{\text{size}}) \quad &\rightarrow \quad \bar{V} = \frac{r_T(1-f_{\text{size}})}{\beta} \\
\beta\bar{V}\bar{T} = \frac{n_E}{\tau_E} A_E \bar{E}_1 \quad &\rightarrow \quad \bar{E}_1 = \frac{\beta\bar{V}\bar{T}\tau_E}{n_E A_E} = \frac{r_T(1-f_{\text{size}})\bar{T}\tau_E}{n_E A_E} \\
\bar{E}_{i-1} = A_E \bar{E}_i \quad &\rightarrow \quad \bar{E}_i = \frac{\beta\bar{V}\bar{T}\tau_E}{n_E A_E^i} = \frac{r_T(1-f_{\text{size}})\bar{T}\tau_E}{n_E A_E^i} \\
\frac{n_E}{\tau_E}\bar{E}_{n_E} = \frac{n_I}{\tau_I} A_I \bar{I}_1 \quad &\rightarrow \quad \bar{I}_1 = \frac{\tau_I n_E}{\tau_E n_I A_I}\bar{E}_{n_E} = \frac{\beta\bar{V}\bar{T}\tau_I}{n_I A_E^{n_E} A_I} = \frac{r_T(1-f_{\text{size}})\bar{T}\tau_I}{n_I A_E^{n_E} A_I} \\
\bar{I}_{i-1} = A_I \bar{I}_i \quad &\rightarrow \quad \bar{I}_i = \frac{\beta\bar{V}\bar{T}\tau_I}{n_I A_E^{n_E} A_I^i} = \frac{r_T(1-f_{\text{size}})\bar{T}\tau_I}{n_I A_E^{n_E} A_I^i}
\end{aligned}$$

where

$$A_E = 1 - \frac{r_E(1-f_{\text{size}})\tau_E}{n_E} \qquad\qquad A_I = 1 - \frac{r_I(1-f_{\text{size}})\tau_I}{n_I} \ .$$

We find that

$$\begin{aligned}
\bar{E} = \sum_{i=1}^{n_E} \bar{E}_i = \sum_{i=1}^{n_E} \frac{\beta\bar{V}\bar{T}\tau_E}{n_E A_E^i} = \frac{\beta\bar{V}\bar{T}\tau_E}{n_E}\frac{A_E^{n_E}-1}{A_E^{n_E}(A_E-1)} = \frac{r_T(1-f_{\text{size}})\bar{T}\tau_E}{n_E}\frac{A_E^{n_E}-1}{A_E^{n_E}(A_E-1)} \\
\bar{I} = \sum_{i=1}^{n_I} \bar{I}_i = \sum_{i=1}^{n_I} \frac{\beta\bar{V}\bar{T}\tau_I}{n_I A_E^{n_E} A_I^i} = \frac{\beta\bar{V}\bar{T}\tau_I}{n_I A_E^{n_E}}\frac{A_I^{n_I}-1}{A_I^{n_I}(A_I-1)} = \frac{r_T(1-f_{\text{size}})\bar{T}\tau_I}{n_I A_E^{n_E}}\frac{A_I^{n_I}-1}{A_I^{n_I}(A_I-1)}
\end{aligned}$$

by utilizing the fact that

$$\sum_{i=1}^{n} \frac{1}{A^n} = \frac{A^n - 1}{A^n(A-1)} \ .$$

Expressing parameters τ_I, p and β as a function of other parameters as was done for the NDP model above, we get:

$$\tau_I = \frac{f_{\text{infec}}}{(1 - f_{\text{infec}}) r_T (1 - f_{\text{size}})} - \tau_E \tag{5.4}$$

$$p = \frac{c\bar{V}}{f_{\text{size}} T_{\max} (1 - f_{\text{size}})(1 - f_{\text{infec}}) r_T \tau_I} \tag{5.5}$$

$$\beta = \frac{r_T \ (1 - f_{\text{size}})}{\bar{V}} \tag{5.6}$$

Chapter 6

Kinetics of the γ-model

In Chapter 4, we introduced a new model, the γ-model, for HCV infection kinetics, which includes an eclipse phase, and flexible delay distributions. This model was developed to better account for known biological properties of the infection and the liver. We saw specifically, in Chapter 3, that in order to model an eclipse phase appropriately, a delay prior to virus release is required, and the transition out of the infectious phase might be modeled by either a delayed (e.g. gamma distribution) or an exponential distribution.

In this chapter, we explore the implications of the additions of delays in the γ-model on HCV VK under antiviral therapy. To simplify the comparison of the different implementations of the eclipse and infectious phase delays, we enforce the following biologically realistic constraints on all models:

$f_{\mathbf{size}} = 0.95$: the infected liver is 95% the size of the uninfected liver;

$T_{\mathbf{max}} = 10^{11}$ cells**:** the susceptible cell population is set to that of an average human liver; and

$f_{\mathbf{infec}} = 0.1$ **or** 0.9**:** either 10% or 90% of the liver is infected, to sample both ends of the values typically reported in the literature.

In addition, a number of parameters were fixed based on their approximately known

values:

$\bar{V} = 10^{6.4}$ **RNA**/mL**,** the median value of the steady-state virus concentration found in the plasma of chronically HCV-infected patients (ranges from 10^4–10^8 RNA/mL) [16].

$c = 5$ d^{-1}**,** the average rate of virus clearance in patients. This value was estimated during liver transplant, where HCV in serum was measured to decay at a rate of 3–22 d^{-1} (HCV virus elimination half life of 2–5.2 h) [28, 62].

$r_T = r_E = 0.12$ d^{-1}**,** the uninfected hepatocyte regeneration rate estimated by fitting data from healthy liver resection in Section 3.2. In models containing an eclipse phase (E), we assume the newly infected eclipse cells can regenerate at the same rate as uninfected hepatocytes ($r_E = r_T$).

$r_I = 0.05$ d^{-1}**,** the infected hepatocyte regeneration rate estimated by fitting data from chronic hepatitis liver resection in Section 3.2.

$\tau_E = 8$ d**,** a value chosen not based on specific biological knowledge, but rather to make the eclipse phase sufficiently long that it can have a significant effect on the VK for the purpose of exploring what that effect might be.

Fixing these different values, together with the constraint equations from Chapter 5, enable us to compute β, p and τ_I for each model in steady state, and readily compare their behaviour under simulated antiviral therapy.

6.1 Impact of the eclipse phase on HCV VK

In the γ-model, we have implemented an eclipse phase between the moment of cell infection and when the cell starts to release virus. Here the influence of this new addition on HCV VK under treatment is studied. Three models are considered and used to compare

	Fixed parameters					Computed parameters		
Model	f_{inf}	r_T d^{-1}	r_E d^{-1}	r_I d^{-1}	τ_E d	p $\frac{\text{RNA}}{\text{mL}\cdot\text{d}\cdot\text{cell}}$	β $\frac{\text{mL}}{\text{RNA}\cdot\text{d}}$	τ_I d
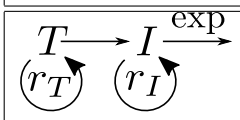	10%	0.12	–	0.05	–	1.32e-3	2.39e-9	17.7
$(n_I = 1)$	90%	0.12	–	0.05	–	1.47e-4	2.39e-9	315
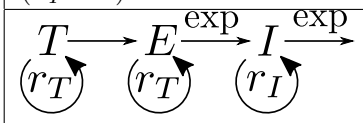	10%	0.12	0.12	0.05	8	2.42e-3	2.39e-9	9.40
$(n_E = 1, n_I = 1)$	90%	0.12	0.12	0.05	8	1.47e-4	2.39e-9	312
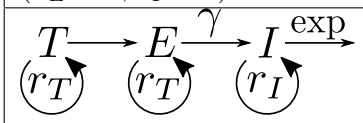	10%	0.12	0.12	0.05	8	2.37e-3	2.39e-9	9.60
$(n_E = 36, n_I = 1)$	90%	0.12	0.12	0.05	8	1.47e-4	2.39e-9	312

Table 6.1: **Exploring various implementations of the eclipse phase.** We set $T_{\max} = 10^{11}$ cells, $f_{\text{size}} = 95\%$, and fix $c = 5/\text{d}$, $\bar{V} = 10^{6.4}$ RNA/mL. For all models, p, β, and τ_I were computed from the fixed parameters and constraints.

their parameter predictions under constraints, and their HCV VK profiles. These models differ in whether they incorporate an eclipse phase, and if so, what distribution is used to implement the time spent by cells in this phase. The three models are shown in Table 6.1 along with their associated parameters.

The first model is a typical ODE HCV model wherein newly infected cells immediately begin producing virus (no eclipse phase). It incorporates target cells, infectious cells and HCV. It is assumed that, there is no production of hepatocytes due to cell migration such that hepatocyte replenishment by cell migration is neglected (i.e., $s = 0$), is neglected. Also the target cell death is neglected because it is assumed to be much smaller than the rate of infection (i.e., $1/\tau_T = 0$). The uninfected and infected hepatocytes are replicated from existing hepatocytes, which will regenerate at rates r_T and r_I, respectively. The second model is another ODE model, but with an exponentially-distributed ($n_E = 1$) eclipse phase between the moment of cell infection and the release of new virions. The third model is constructed under the same assumptions, and it only differs from the

second model in that its eclipse phase is gamma-distributed, rather than exponentially-distributed, with standard deviation $\tau_E/6$ ($n_E = 36$). In all three models, an exponential-distribution is used to model infectious cell lifespan so as to study only the influence of the eclipse phase and its associated distribution.

Computed parameters in Table 6.1 are compared to explore the effect of model variation on steady state parameter predictions, while imposing the constraints listed above. Parameters p and β are essentially the same in all three models, but τ_I varies. Note, however, that the value of τ_I in the first model, which does not include an eclipse phase is approximately equal to $\tau_E + \tau_I$ in the second and third model, which do incorporate an eclipse phase. Therefore, the addition of an eclipse phase for equivalent parameters leaves the amount of time spent by a cell in an infected state (E and I) unchanged, but reduces the amount of time spent by a cell in the productively infectious state (I). When f_{infec} is large, all models predict the same parameters, and the relationship between f_{infec} and τ_I presented in Chapter 5 imposes a long infectious cell lifespan, τ_I, in both models.

Figure 6.1 shows that the incorporation of eclipse phase and lifespan distribution leads to different dynamics for simulated antiviral treatment. All models have the same first phase decay independent of model variation. This confirms that the first phase decay mainly depends on the viral clearance rate, c, and antiviral efficacy, ε, even when an eclipse phase is introduced, irrespective of the distribution used for the duration of that eclipse phase. The models do, however, differ in their subsequent decay phases depending on both whether there is an eclipse phase or not, and whether that eclipse phase follows an exponential or a gamma distribution. Both models with an eclipse phase have a steeper last phase HCV decline. Note, however, that the constraints imposed on model parameters lead to shorter infectious cell lifespans. This supports that the VK decline in the last phase does depends on the infectious cell lifespan, τ_I.

The model with a gamma-distributed eclipse phase creates a shoulder, and changes the VK decline profile from a biphasic to a triphasic decay. Also it has a steeper last

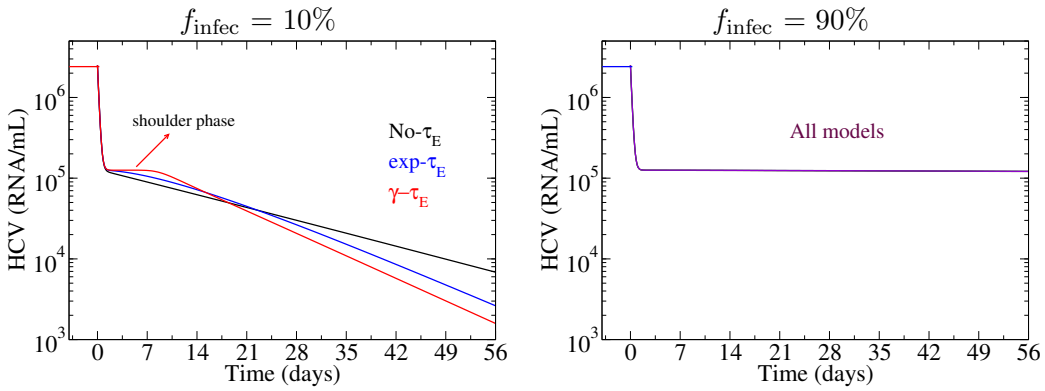

Figure 6.1: **The effect of different delays for the eclipse phase.** An antiviral (95% efficacy) was applied to p (e.g., IFN-α). All models have the same first phase decay. Models with eclipse phase (blue and red lines) have a steeper second phase HCV decline because imposed constraints lead to shorter infectious cell lifespan τ_I. A gamma-distributed eclipse phase (γ-τ_E) creates a shoulder phase and a steeper second phase decline compared to an exponentially-distributed one. When τ_I is long ($f_{\text{infec}} = 90\%$), all models exhibit the same flat VK.

phase decline. This difference means probably that the exp-τ_E model ($n_E = 1$) decay depends on both τ_E and τ_I while a gamma-distributed model decay depends only on τ_I with value 9.6 d. When f_{infec} is large (90%), the constraints impose a long infectious cell lifespan. The long lived infectious cell population remains constant and therefore, all models exhibit the same flat VK.

6.2 Impact of infectious cell delay distributions on HCV VK

In this section, the effect of the infectious lifespan distribution on HCV VK under antiviral therapy is studied by comparing two models. Both models have a gamma-distributed eclipse phase ($n_E = 36$), and differ in having either an exponentially-distributed ($n_I = 1$) or a gamma-distributed ($n_I = 36$) infectious cell lifespan. The same constraints as before are applied, plus the eclipse phase lifespan is fixed to $\tau_E = 0.33$ d, the minimum observed eclipse phase in vitro [36, 79].

	Fixed parameters					Computed parameters		
Model	f_{inf}	r_T d^{-1}	r_E d^{-1}	r_I d^{-1}	τ_E d	p $\frac{\text{RNA}}{\text{mL}\cdot\text{d}\cdot\text{cell}}$	β $\frac{\text{mL}}{\text{RNA}\cdot\text{d}}$	τ_I d
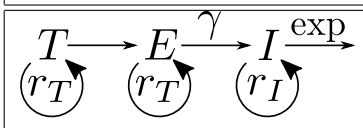	10%	0.12	0.12	0.05	0.33	1.35e-3	2.39e-9	17.7
$(n_E = 36, n_I = 1)$	90%	0.12	0.12	0.05	0.33	1.47e-4	2.39e-9	316
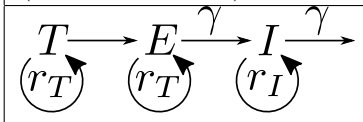	10%	0.12	0.12	0.05	0.33	1.35e-3	2.39e-9	17.7
$(n_E = 36, n_I = 36)$	90%	0.12	0.12	0.05	0.33	1.47e-4	2.39e-9	609

Table 6.2: **Exploring various implementations of the infectious cell lifespan.** We set $T_{\text{max}} = 10^{11}$ cells, $f_{\text{size}} = 95\%$, $c = 5/\text{d}$, $\bar{V} = 10^{6.4}$ RNA/mL. For all models, p, β, and τ_I were computed from the fixed parameters and constraints.

As in the previous section, model parameter predictions under constraints and their HCV VK profiles are compared. Computed parameters in Table 6.2 yield identical values for p and β. The infectious cell lifespan, τ_I, at $f_{\text{infec}} = 10\%$ is the same for both models, but it varies at $f_{\text{infec}} = 90\%$. The first model, with an exponentially-distributed infectious cell lifespan, give smaller τ_I value. The second model, with a gamma-distributed infectious lifespan, gives a very long lifespan, almost twice than of the first model. Irrespective of the distribution, however, we see that, as in the previous section, a large f_{infec} (90%) in these models under our imposed constraints requires a long infectious cell lifespan, leading to a flat VK.

Although the model delay assumptions did not change the steady state parameter predictions at $f_{\text{infec}} = 10\%$, it did affect the VK profile under treatment. Figure 6.2 shows that distinguishable second phase decays are produced by the different infectious lifespan distributions. The model with gamma-distributed infectious cell lifespans (γ-τ_I) has a steeper second phase HCV decline because almost all cells move out of the infectious phase around the mean time, τ_I, and long lived cells are avoided. Both models VK profile are identical at $f_{\text{infec}} = 90\%$ (i.e., very long τ_I).

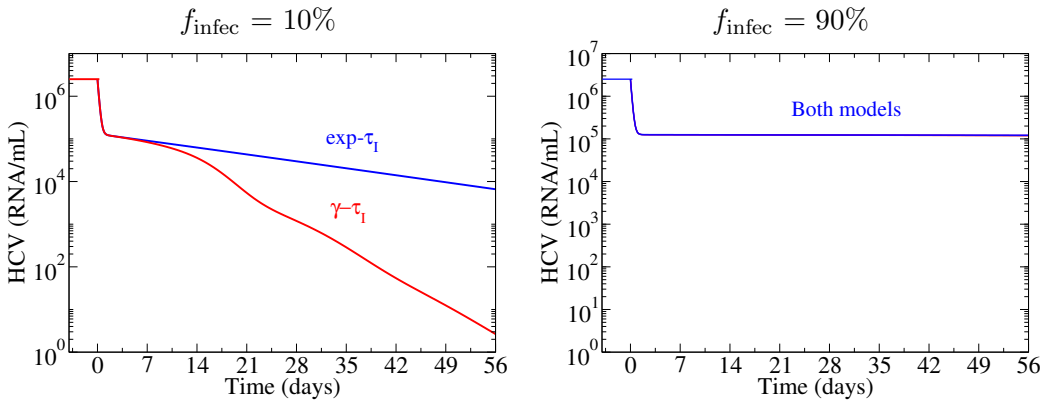

Figure 6.2: **The effect of different infectious phase delays.** An antiviral (95% efficacy) was applied to p (e.g., IFN-α). Exponentially-distributed (exp-τ_I) and gamma-distributed (γ-τ_I) infectious cell lifespans yield the same first phase decay. However, γ-τ_I leads to a steeper 2nd phase HCV decline because almost all cells move out of the infectious phase rapidly. When τ_I is long ($f_{\text{infec}} = 90\%$), both models have same VK.

Based on the discussion in Chapter 3, the transition out of the infectious phase might be modeled by either a gamma or an exponential distribution. Since the NDP model is an exponentially-distributed model, in the next chapter we will be doing fits to patient data with the new γ-model (now fixing $n_E = n_I = 36$, to achieve gamma-distributed eclipse and infectious phases) and the NDP model to hopefully determine which distribution represents infected cell loss most accurately.

6.3 Exploring parameter variations

The dynamics that each mathematical model predicts changes as each parameter in the model is varied. For example, in previous sections, we saw that a longer infectious cell lifespan leads to a smaller viral decay slope. To understand the effect of each parameter on various viral decay phases under therapy, we have explored parameter variations in the γ and NDP models (Figures 6.3–6.8). In both models, parameters are fixed to the above-mentioned reasonable values, and then each parameter is varied individually. Parameters p, β and τ_I are computed to satisfy the constraints.

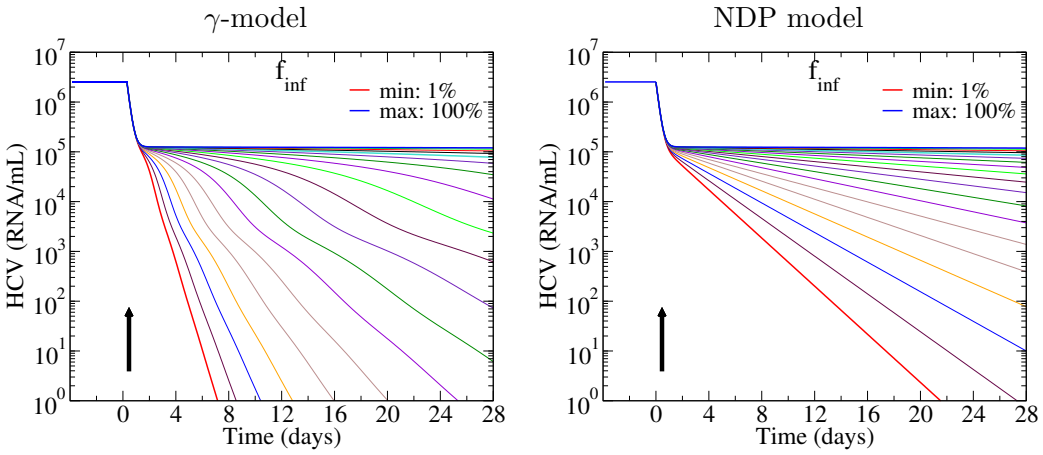

Figure 6.3: **The effect of f_{infec} on HCV VK under treatment.** As the fraction of liver infected increases ($f_{\text{infec}} = 1\% \rightarrow 100\%$) in both the γ (left) and NDP (right) models, the constraints force the infectious cell lifespan to increase ($\tau_I = 1$ d $\rightarrow \sim 350$ d), causing the rate of decay in the second phase to decrease. When the infectious cell lifespan is very large, HCV titer rapidly settles into a new lower level where the long-lived infectious cell population remains constant.

As we saw in the previous two sections, increasing f_{infec} in both models increases the infectious cell lifespan which, in turn, decreases the rate of decline in the second phase (Figure 6.3). When f_{infec} =1%, $\tau_I = 1$ day, and when $f_{\text{infec}} \sim 100\%$, $\tau_I \sim 350$ days. When the infectious cell lifespan is very large, HCV titer rapidly settles into a new lower steady state and the long-lived infectious cell population remains constant over the duration of the simulation. This is also true when f_{size} is increased, or the regeneration rate of target (r_T) or infectious (r_I) cells are decreased in both models (Figure 6.4) as one expected from equations (5.1) and (5.4).

Increasing the antiviral efficacy of IFN in blocking new virion production, ε, in the γ-model (Figure 6.5) increases both the level to which virus concentration drops (first phase) and the rate of viral decay in second phase. However, in the NDP model, only the first phase decay is influenced by ε. An antiviral efficacy on blocking new infection, η (e.g. like RBV) shows only a small influence on the viral kinetic profile (Figure 6.6). In the γ-model, for example, as RBV efficacy increases, it increases the rate of decay

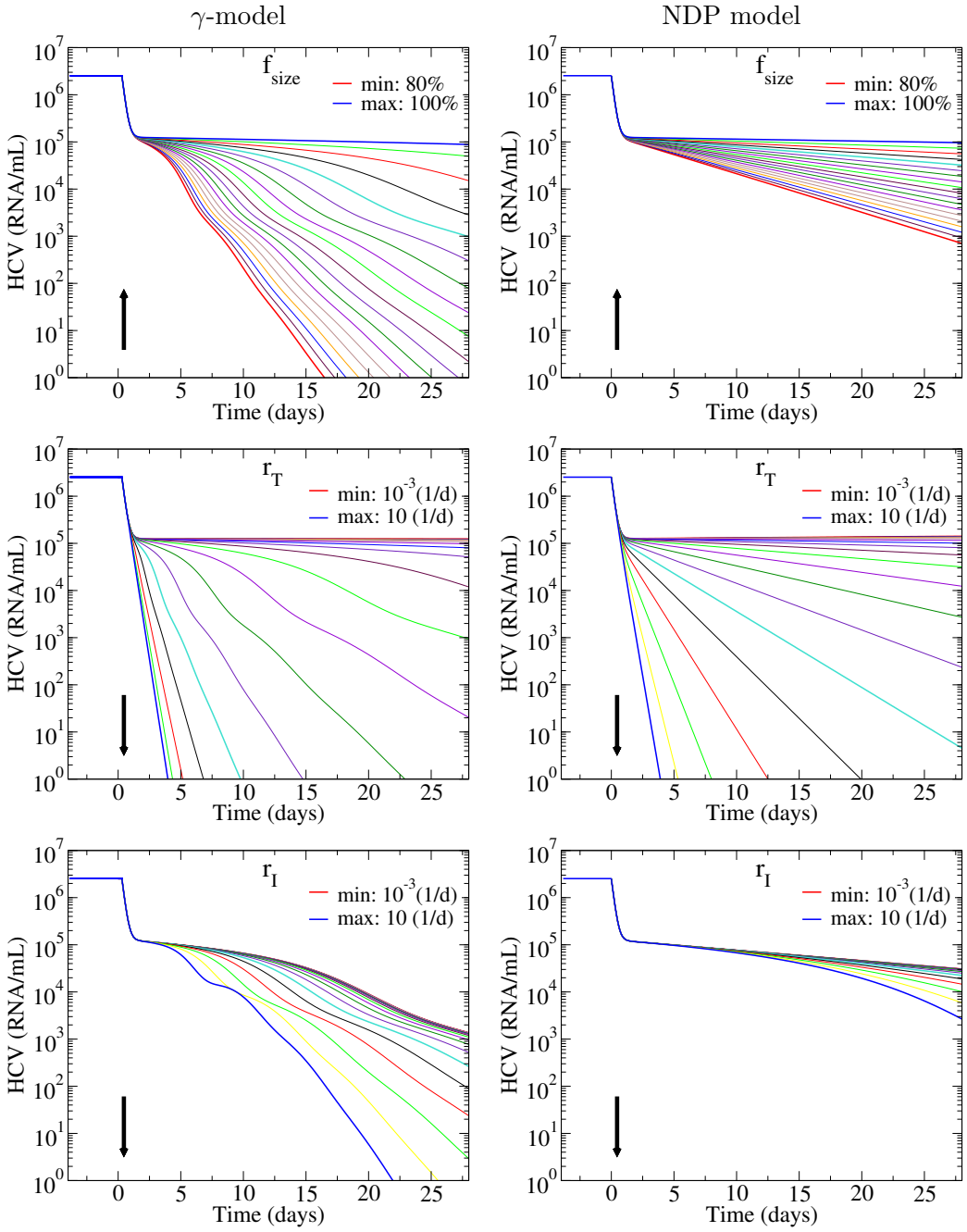

Figure 6.4: **The effect of f_{size}, r_T and r_I on HCV VK under treatment.** Increase of f_{size} (first row) in γ-model (left) and NDP model (right) decreases rate of the second phase decay. Also, a decrease of the regeneration rate of target cells, r_T, (second row) and infectious cells, r_I, (third row) showed same results.

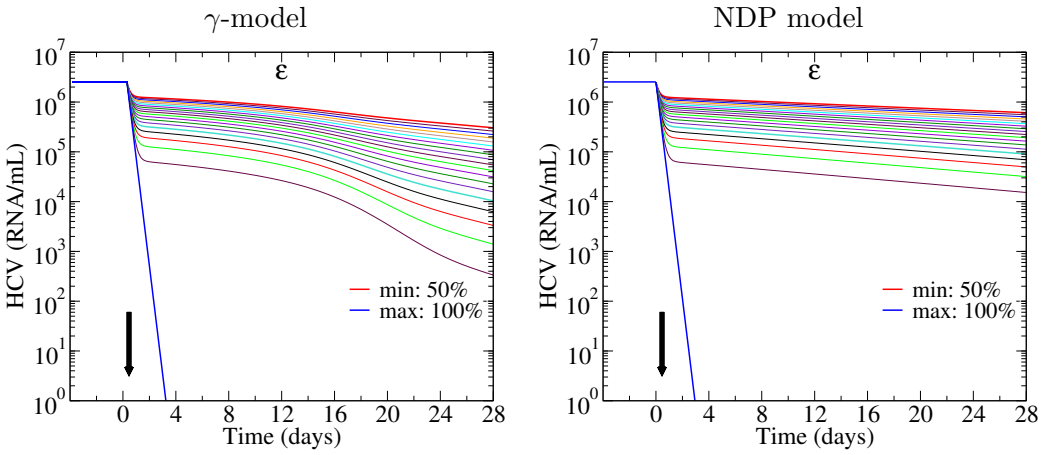

Figure 6.5: **The effect of interferon (IFN) antiviral efficacy on HCV VK.** Increase of IFN antiviral efficacy on blocking virus production, p, in the γ-model (left) increases the rate of decay in both the first and second phases, however in the NDP model (right) the second phase decay is the same.

in the third phase. Cells begin to die and are replaced by uninfected cells protected by RBV+IFN. In the NDP model, with exponentially-distributed cell lifespans, RBV has no effect because the long-lived infectious cells are not being replaced by susceptible cells, and hence cannot benefit from the protection afforded by RBV.

Increasing the viral clearance rate, c, increases the rate of decay in the first phase, just as IFN treatment, ε. However, unlike ε, it has little effect on the second phase (Figure 6.7).

Increasing τ_E in the γ-model creates a VK shoulder and changes VK from a biphasic to a triphasic decay. To verify that only eclipse phase length is causing this conversion from a biphasic to a triphasic VK, the exp-τ_I and γ-τ_I models from Section 6.2 with a gamma-distributed eclipse phase were compared. Figure 6.8 shows that increasing τ_E increases the shoulder length in both models. Due to our constraints, as τ_E increases (from 2.4h to 17d), τ_I is forced to decrease (17d to 2.4h). For large τ_E, i.e., small τ_I, the upper lines are the same in both models, however as τ_E decreases, and τ_I increases, the gamma-distributed lifespan results in a more abrupt viral decay.

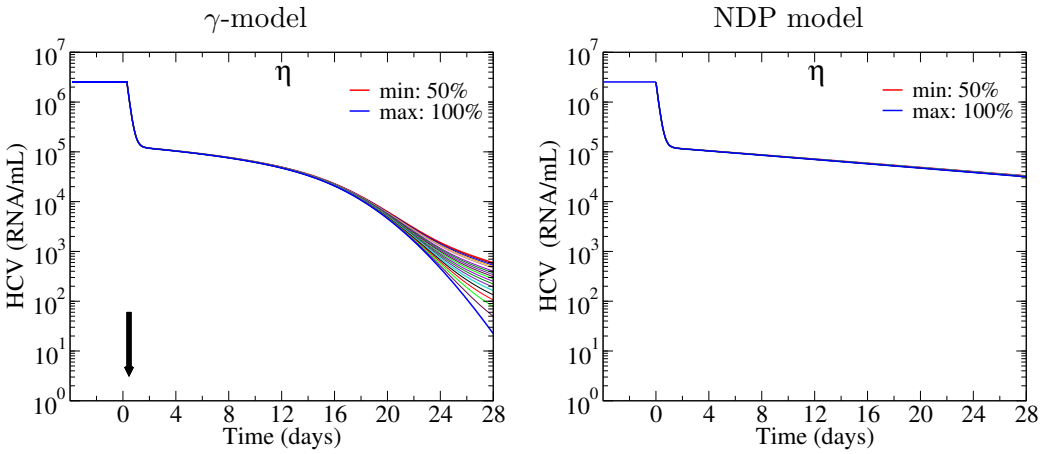

Figure 6.6: **The effect of ribavirin (RBV) efficacy on HCV VK.** Increase of RBV efficacy at blocking new infection, β, in the γ-model (left) increases the rate of decay in the 3rd phase but has no effect in the NDP model (right) because of the long-lived infectious cells (exponential distribution).

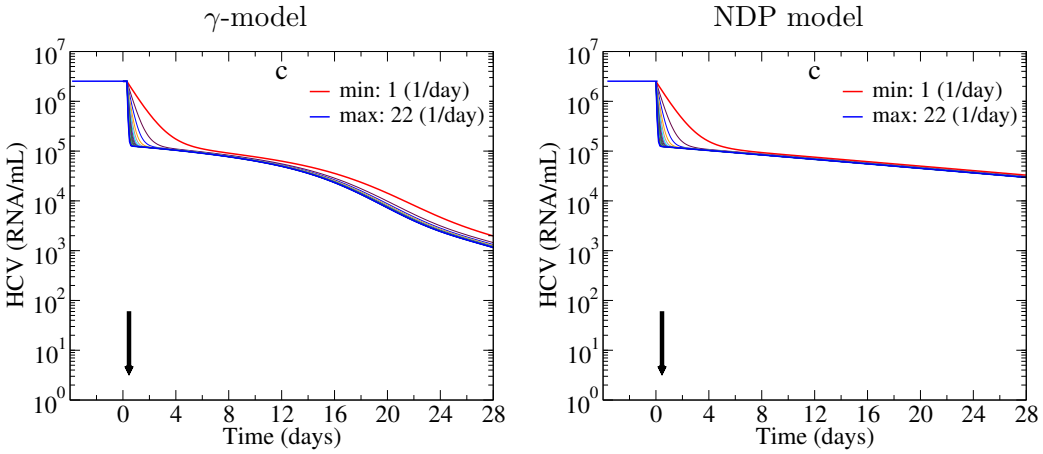

Figure 6.7: **The effect of viral clearance, c, on HCV VK under treatment.** Increasing the rate of viral clearance, c, in both the γ-model (left) and NDP model (right), increases the rate of decay in the first phase, but has little effect on the second phase.

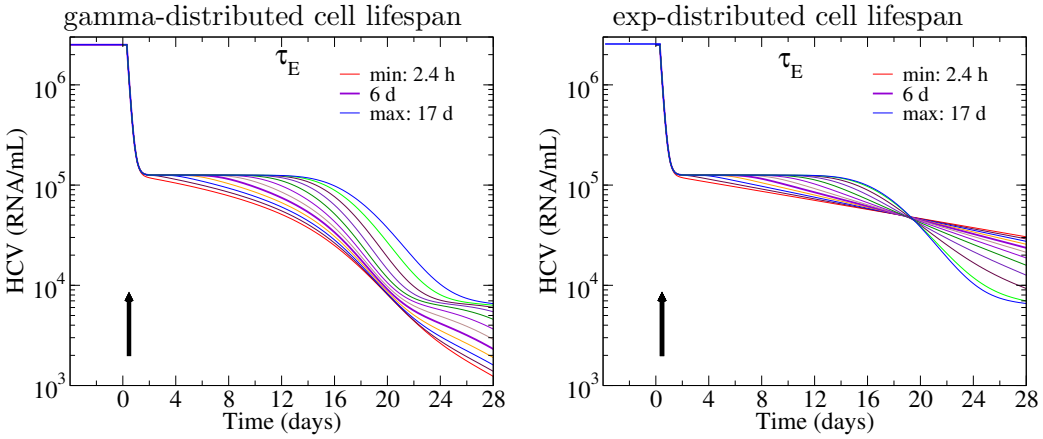

Figure 6.8: **The effect of the eclipse phase duration on HCV VK under treatment.** Increasing the duration of the eclipse phase, τ_E, creates a VK shoulder and changes the VK from a biphasic to a triphasic decay. When the infectious cell lifespan is gamma-distributed (left), viral decay is more abrupt compared to exponentially-distributed cell lifespans (right).

Chapter 7

Confronting the models to patient data

To validate a mathematical model, it is important to compare its predictions to experimental data. We therefore searched the literature for clinical studies that included frequent serum sampling from humans chronically infected with HCV undergoing antiviral therapy. The most extensive data sets available are for treatment with either interferon (IFN) alone, or in combination with ribavirin (IFN+RBV). Treatment with IFN includes daily or thrice weekly doses of IFN. In some patients, in addition to IFN, RBV is administered daily. The approximate duration of HCV treatment with IFN or IFN+RBV is at least 24 weeks and, depending on the HCV genotype or patient tolerance, can lasts upwards of 72 weeks [6,78]. Blood samples from chronically infected HCV patients undergoing antiviral therapy are typically collected every few hours during the first 2 days, then daily for 2 weeks [49], and then at decreasing frequencies thereafter which differ for each study, with the end of collection typically coinciding with the end of therapy. From these blood samples, the levels of HCV load in the blood is determined for each patient via polymerase chain reaction (PCR) or reverse transcriptase PCR (RT-PCR) which yields the HCV viral load in units of RNA/mLof blood serum.

In recent years, a number of studies have also evaluated the effect of direct acting antivirals (DAAs) [71, 72]. However, since DAAs often give rise to antiviral resistance over the course of treatment, they require that drug resistance be incorporated into the models. Since our aim is simply to compare our two models in the simplest possible case, we focus only on HCV VK from patients treated with either IFN or IFN+RBV.

In this chapter, we fit both the γ and NDP models to HCV viral load measurements for individual patients undergoing antiviral therapy, while imposing some constraints, and extract the set of unknown parameters. Although fits of the NDP model to these data sets have already been performed in prior work, here we repeat these fits but this time we enforce the same constraints applied to the γ-model. This allows us to utilize additional information (discussed above) to improve the fits and makes a fair comparison between the model types. We first present details of the fitting procedure, including the method of fitting, how the first phase decay is account for, and how constraints are applied to the parameters. Finally, we fit both models to patient data in each of the three VK category profiles (biphasic, triphasic, flat partial), and compare the results.

7.1 Methods

7.1.1 Nonlinear regression technique

In order to compare the fits to experimental data, the sum of squared residuals (SSR) is used. This is given by the sum of the squares of the differences between the data points and the estimated model points, which is formulated as:

$$\text{SSR} = \sum_{i=1}^{n} (y_i - f(x_i))^2,$$

where y_i is the experimental data point and $f(x_i)$ is the model-estimated point. The set of parameters for which the SSR is minimized are the best fit parameters. Therefore, a small SSR indicates a good fit of the model to the data [43].

An Octave 3.2.4 (www.octave.org) implementation of the Nelder-Mead method, originally proposed by John Nelder and Roger Mead in 1965 [48], was used to fit the mathematical models to the HCV RNA data, and to estimate the best fit parameter values. In the analysis that follows, the SSR is presented to quantify how well a model represents the experimental data.

7.1.2 Fitting the first phase of viral decay

The consideration of parameter variation in Chapter 6 showed that the first phase of viral decay is indicative of the effectiveness of therapy in blocking viral production (i.e., ε) and the viral clearance rate. This validates the approach taken by the authors of the NDP model in fitting a simpler model to the first phase, as mentioned in Chapter 2. The NDP model assumes that, over the first 2 days of therapy, the number of target and infectious cells remain approximately at their steady state values, $T(t) \approx \bar{T}$ and $I(t) \approx \bar{I}$. In making this assumption, the analytical solution of Eq. (2.2) for $\mathrm{d}V/\mathrm{d}t$ can be found:

$$V(t) = \bar{V}[1 - \varepsilon + \varepsilon \ \mathrm{e}^{-c(t-t_0)}] \tag{7.1}$$

By fitting Eq. (7.1) to the first phase decay in patient data, they were able to estimate the baseline HCV RNA/mL, $\bar{V}$, the delay time, t_0, the antiviral efficacy, ε, and the viral clearance rate, c.

If we consider the first few days of the γ-model dynamics after initiation of therapy (Figure 7.1), we see that some of these simplifying assumptions hold true in the VK (the number of target cells and infectious cells are relatively constant at their steady state values, $T \approx \bar{T}$ and $I \approx \bar{I}$), but the number of eclipse cells declines at a same rate as the virus ($E \neq \bar{E}$). Importantly, however, the eclipse cell population does not appear in Eq. (4.1) for $\mathrm{d}V/\mathrm{d}t$, and therefore does not change the analytical solution. Thus, for both

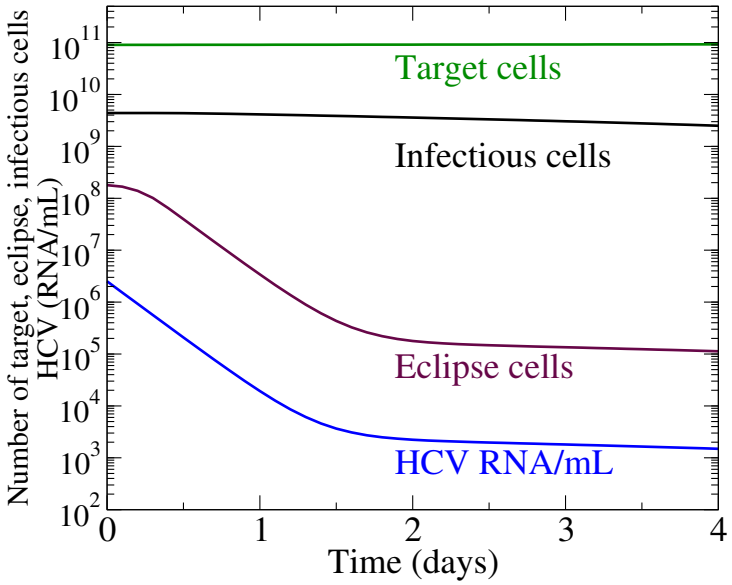

Figure 7.1: **Cell populations in the γ-model, in the first few days after initiation of therapy.** The number of target cells and infectious cells are relatively constant at their steady state values, $T \approx \bar{T}$ and $I \approx \bar{I}$, and the number of eclipse cells decline at a same rate as viral decay under therapy (at rate $c\varepsilon$). Parameters are the same as those presented in Table 6.2 for f_{infec} =10%.

models, we fit Eq. (7.1) to the VK of the first phase and use it to estimate parameters $\bar{V}, t_0$ and the product $c\varepsilon$. We make one slight modification to the procedure used by the NDP authors: We do not estimate c and ε separately in the fit to Eq. (7.1) because parameter variation in Chapter 6 showed that the first phase decay actually depends on $c\varepsilon$, rather than c and ε, such that neither can be determined independently.

7.1.3 Reducing the number of free parameters

The functional form of the observed patient data is relatively simple (see, e.g., Figure 2.6) and only allows for the determination of a small number of parameters. Therefore, it is important that the number of free parameters when fitting the VK profile be as small as possible. Imposing biological constraints and extracting parameters $\bar{V}$ and $c\varepsilon$ from fitting the first phase decay allows us to reduce the number of free parameters in the model.

The γ-model has a total of 13 parameters (r_T, r_E, r_I, τ_E, τ_I, n_E, n_I, β, p, c, $T_{\max}$, ε and η). By fixing the liver size (relative to uninfected) to either $f_{\text{size}} = 90\%$ or 99% and the steady state virus concentration $\bar{V}$ using our fit of the first phase decay, and using the fraction of liver infected, f_{infec}, as a free parameter, three parameters (p, β, τ_I) are replaced (discussed in Chapter 5). Using the biological information presented in Chapter 3, we can fix $T_{\max} = 10^{11}$ cells, $r_T = r_E = 0.12$ d^{-1} and $r_I = 0.05$ d^{-1}. We also fixed $n_E = n_I = 36$. Therefore, the number of free parameters in the γ-model is reduced to 5 (c, ε, η , τ_E and τ_I and f_{infec}).

The NDP model has a total of 11 parameters (r_T, r_I, s, τ_T, τ_I, β, p, c, $T_{\max}$, ε and η). The same constraints are imposed on this model. This model, however, assumes two sources for the replacement of lost hepatocytes: proliferation via parameters r_T and r_I, and migration of cells from other sites via parameter s [18, 19, 22]. Therefore we were not able to use the r_T and r_I values obtained in Chapter 3 in the NDP model and are left with 8 parameters (c, ε, η, r_T, r_I, s, τ_T and τ_I and f_{infec}).

7.2 Biphasic decays

The HCV RNA levels of five HCV-infected patients (patients 15, 16, 23 and 34 from [26] and patient p31 from [63]) treated with IFN+RBV are shown with model fits in Figures 7.2–7.6.

The most important estimated parameter values are given inside the figures. These key parameters are the antiviral efficacies (ε and η), the viral clearance rate (c) and the fraction of liver infected (f_{infec}). But f_{infec} and the infected cell lifespan $\tau_E + \tau_I$ are not independent, one determines the other by the constraints. We also indicate the eclipse and infectious cells lifespan in each figure. The SSR is presented to compare the fits. The remaining parameters, such as the uninfected and infected regeneration rates (r_T, r_E and r_I), the viral production rate (p), new infection rate (β), *de novo* cell growth rate (s) and death rate ($1/\tau_T$), are provide in Appendix A.

Both the γ-model and the NDP model give good fits to biphasic patient data at $f_{\text{size}} = 90\%$ and 99%. At $f_{\text{size}} = 99\%$, the models predicted a smaller fraction of cells infected. Both models give approximately the same IFN efficacy, ε. However the estimated RBV efficacy, η, is very different, indicating that the efficacy of antivirals preventing infection (e.g., RBV) cannot be reliably determined.

A number of points in the individual patient fits are notable. Fits to patient-16 and patient-p31 in Figures 7.3 and 7.5 showed that the γ-model is better fitted to data in the first few days and gives higher antiviral efficacy, ε, which indicates a larger first phase decay. The NDP model estimated a shorter infectious cell lifespan, which makes a steeper second phase but missed few data points in the first few days. In fitting patient-34 (Figure 7.6), the γ-model gives better fit and found $\tau_E = 3$ d, which creates a short shoulder phase and reduces the infectious cells lifespan. As a result, steeper last phase decay is observed.

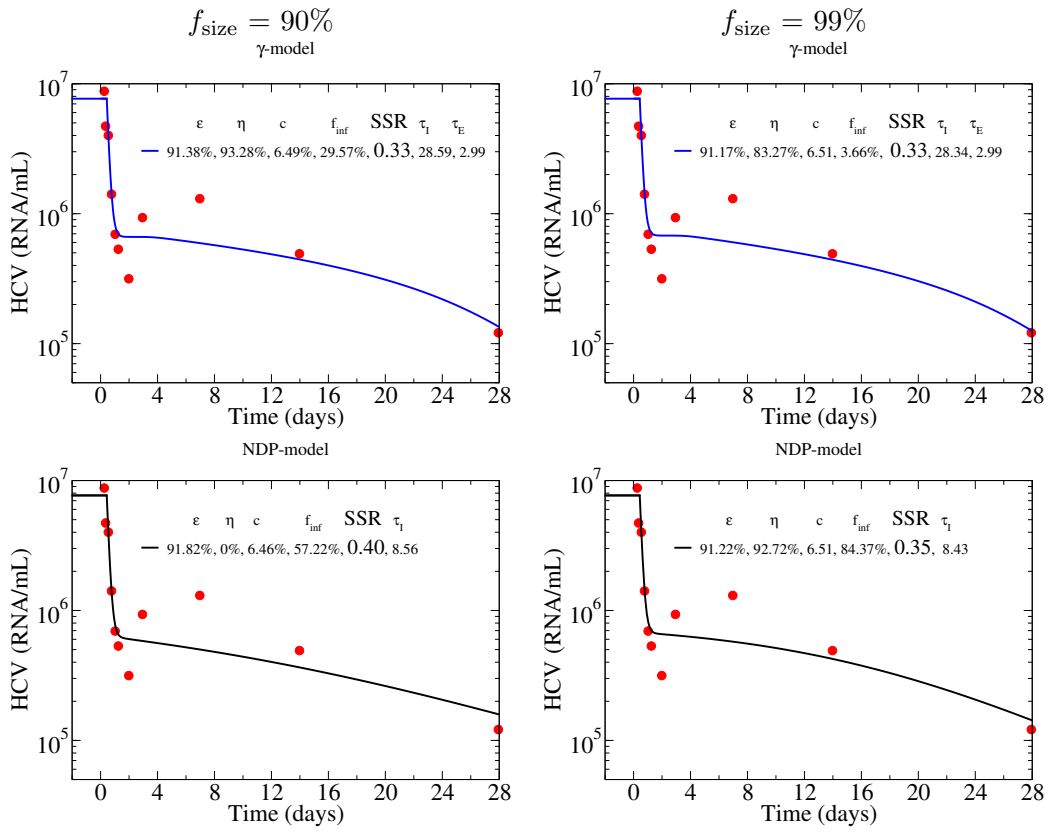

Figure 7.2: **Fits to biphasic decay patient-15 data from Dixit et al. (2004) treated with IFN+RBV.** The γ-model (blue lines) and NDP model (black lines) fits to patient data. In the left column it is assumed that the infected liver size is 90% of its original size, and in the right column $f_{\text{size}} = 99\%$. The steady state viral load is $\bar{V} = 7.68 \times 10^6$ HCV$\frac{\text{RNA}}{\text{mL}}$ and the delay time is $t_0 = 0.43$ d. Other parameter values are shown in Table A.1.

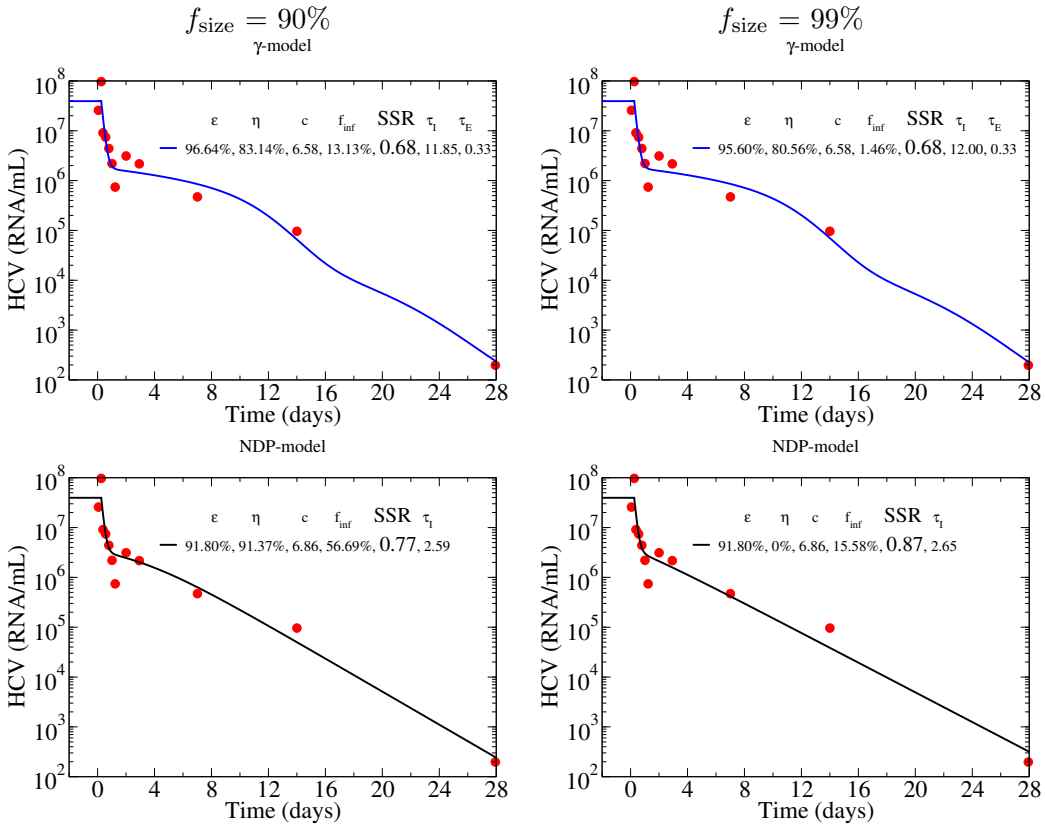

Figure 7.3: **Fits to biphasic decay patient-16 data from Dixit et al. (2004) treated with IFN+RBV.** The first and second row, respectively, show the γ-model (blue lines) and NDP model (black lines) fit to patient data. In the left column it is assumed that the infected liver size is 90% of its original size, and in the right column $f_{\text{size}} = 99\%$. The steady state viral load is $\bar{V} = 3.95 \times 10^7$ HCV$\frac{\text{RNA}}{\text{mL}}$ and the delay time is $t_0 = 0.25$ d. Other parameter values are shown in Table A.2.

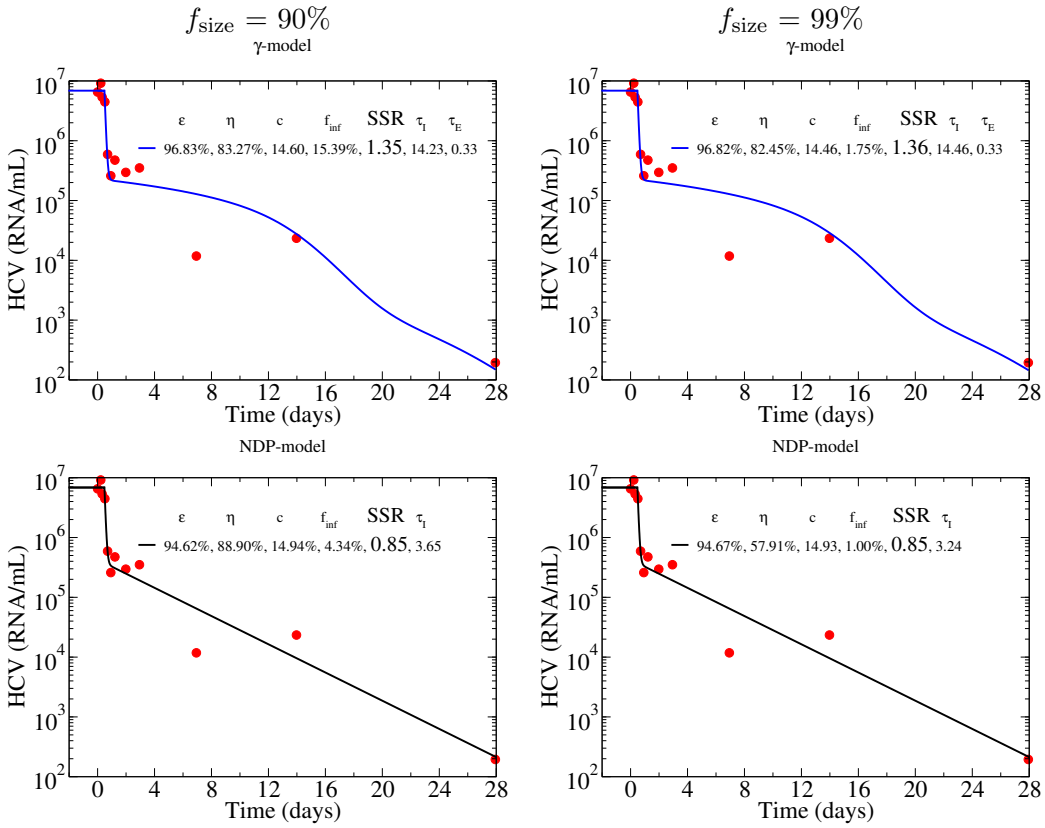

Figure 7.4: **Fits to biphasic decay patient-23 data from Dixit et al. (2004) treated with IFN+RBV.** The first and second row, respectively, show the γ-model (blue lines) and NDP model (black lines) fit to patient data. In the left column it is assumed that the infected liver size is 90% of its original size, and in the right column $f_{\text{size}} = 99\%$. The steady state viral load is $\bar{V} = 6.83 \times 10^6$ HCV$\frac{\text{RNA}}{\text{mL}}$ and delay time is $t_0 = 0.48$ d. Other parameter values are shown in Table A.3.

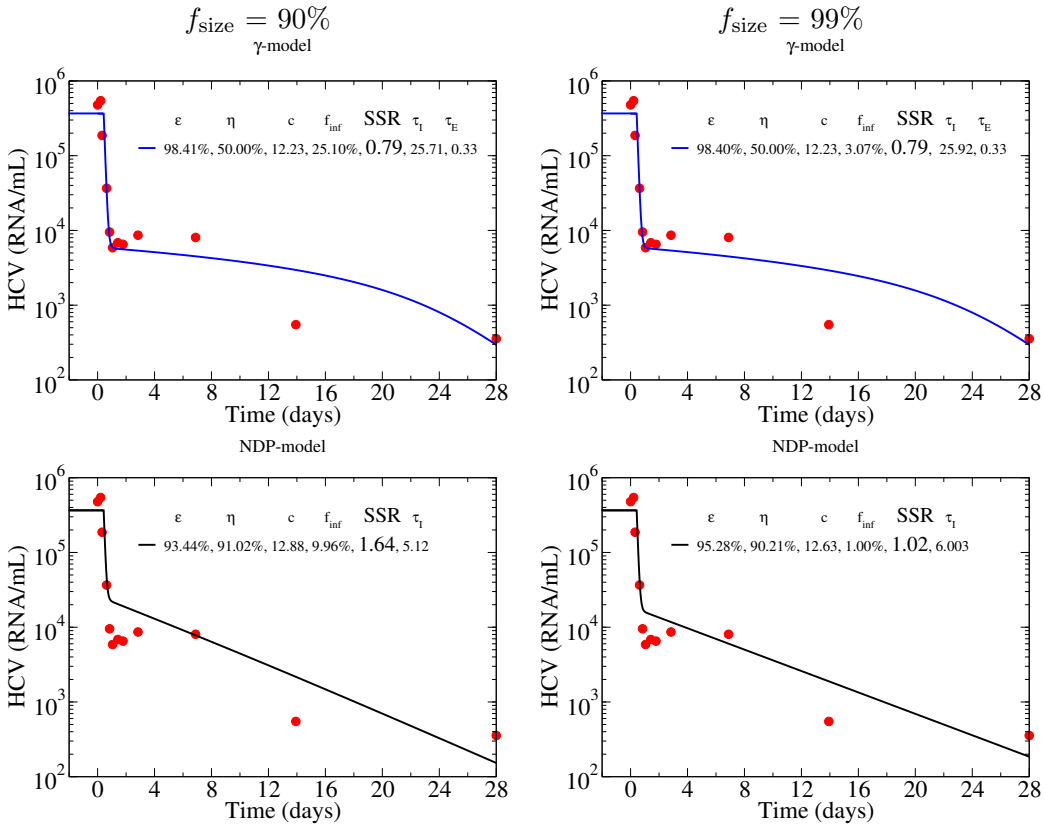

Figure 7.5: **Fits to biphasic decay patient-p31 data from Ribeiro et al. (2003) treated with IFN+RBV.** First and second row, respectively, show the γ-model (blue lines) and the NDP model (black lines) fit to patient data. In the left column it is assumed that the infected liver size is 90% of its original size, and in the right column $f_{\text{size}} = 99\%$. The steady state viral load is $\bar{V} = 3.64 \times 10^5$ HCV$\frac{\text{RNA}}{\text{mL}}$ and the delay time is $t_0 = 0.42$ d. Other parameter values are shown in Table A.4.

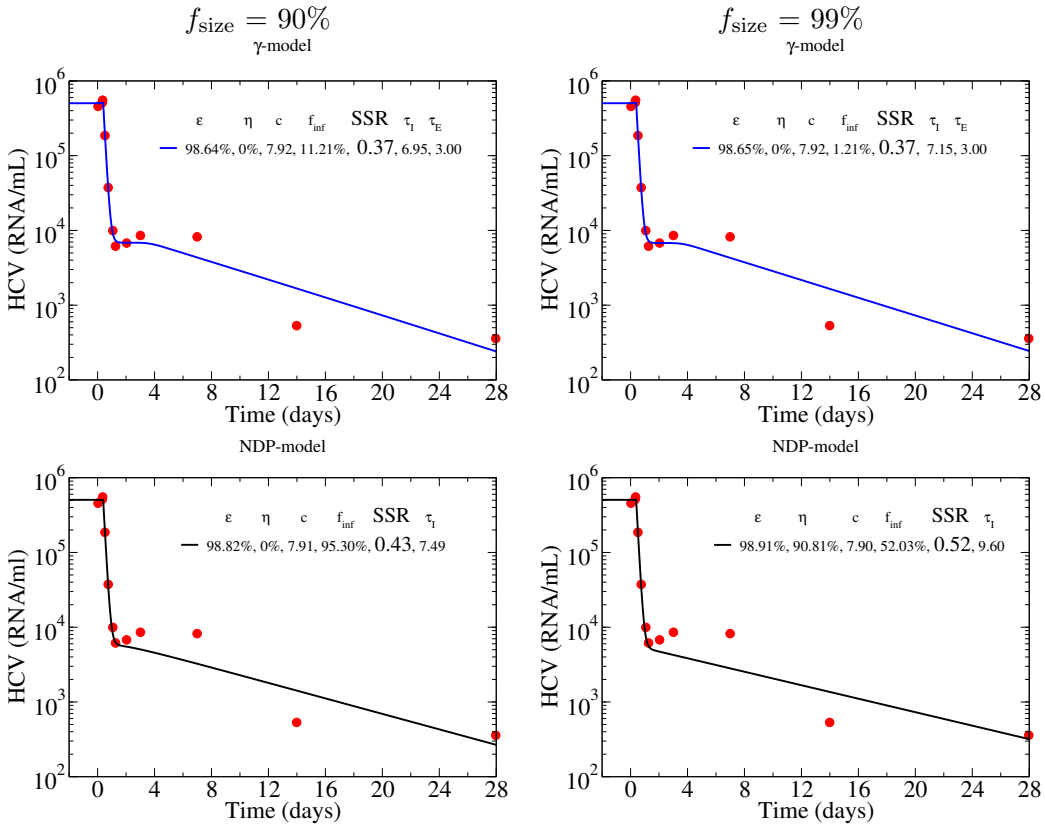

Figure 7.6: **Fits to biphasic decay patient-34 data from Dixit et al. (2004) treated with IFN+RBV.** The first and second row, respectively, show the γ-model (blue lines) and NDP model (black lines) fit to patient data. In the left column it is assumed that the infected liver size is 90% of its original size, and in the right column $f_{\text{size}} = 99\%$. The steady state viral load is $\bar{V} = 5.05 \times 10^5$ HCV$\frac{\text{RNA}}{\text{mL}}$ and the delay time is $t_0 = 0.39$ d. Other parameter values are shown in Table A.5.

7.3 Triphasic decays

In this section, we consider the γ-model and NDP model fits to experimental data with a triphasic VK profile. Recall from Section 2.2 that the NDP model was able to describe a shoulder phase by assuming a very large fraction of liver infected, and high regeneration rates. Here, we show that the γ-model is able to produce a shoulder in the same way, using the regeneration term, but it is also able to produce a shoulder phase by having a long, gamma-distributed, eclipse phase which does not require that such a high fraction of the liver be infected. In Figures 7.7 and 7.8, the bottom two plots show fits of the first type and the top shows fits of the latter type.

Models fits to patient-2B data from [31] and patient-T data from [61] treated with IFN, in Figures 7.7 and 7.8, show that both models do equally well in fitting triphasic patient data, and predict similar IFN efficacy and clearance rate (in their best fits). To produce a shoulder phase with the γ-model with a large fraction of liver infected ($I \gg T$) it was necessary to ignore our previous estimates of hepatocyte regeneration rates and allow r_T and r_I to take significantly larger values. However, when the γ-model captures the shoulder phase by enforcing a long-lasting eclipse phase, the regeneration rates were fixed to realistic biological values and consequently a smaller f_{infec} is estimated.

The NDP model could only produce a shoulder when f_{size} was small and f_{infec} was very large. At large $f_{\text{size}} = 99\%$, a smaller f_{infec} must be imposed to satisfy the constraints, meaning that the population of infectious cells is not much higher than the uninfected cell population, and so a shoulder phase cannot be obtained.

7.4 Flat partial decays

A flat partial decay after antiviral initiation has been observed in a few patients. Here, both the γ-model and NDP model are fitted against experimental data with a flat partial VK profile. Patient-24 data from [26], treated with IFN+RBV, is fitted with both models

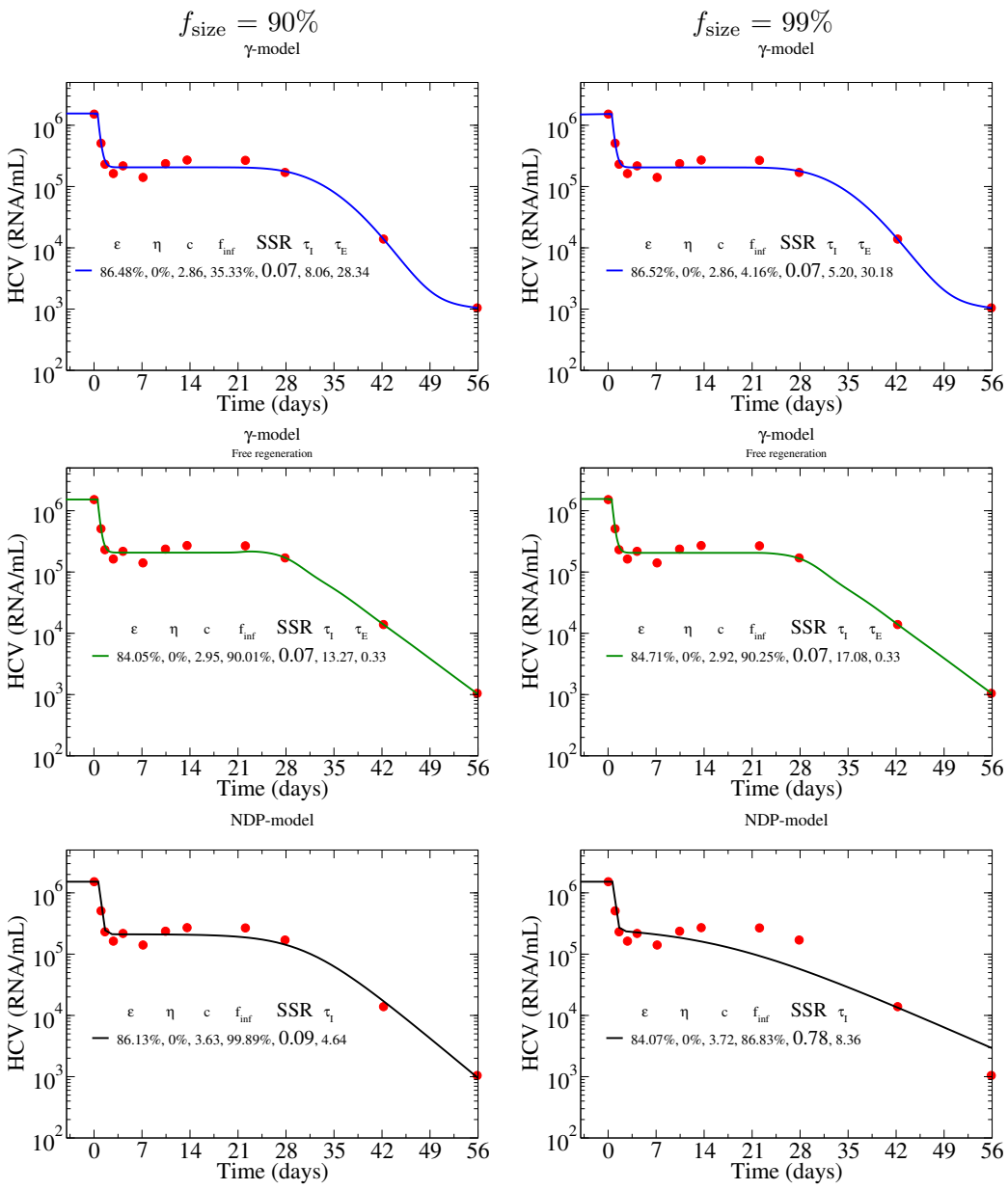

Figure 7.7: **Fits to triphasic decay patient-2B data from Hermann et al. (2003) treated with IFN.** The top rows show the γ-model fit to the patient data with the regeneration rates either constrained (blue lines) or free (green lines). The bottom row show the NDP model (black lines) fit. In the left column it is assumed that the infected liver size is 90% of its original size, and in the right column $f_{\text{size}} = 99\%$. The steady state viral load is $\bar{V} = 1.52 \times 10^6$ HCV$\frac{\text{RNA}}{\text{mL}}$ and the delay time is $t_0 = 0.62$ d. Other parameter values are shown in Table A.6.

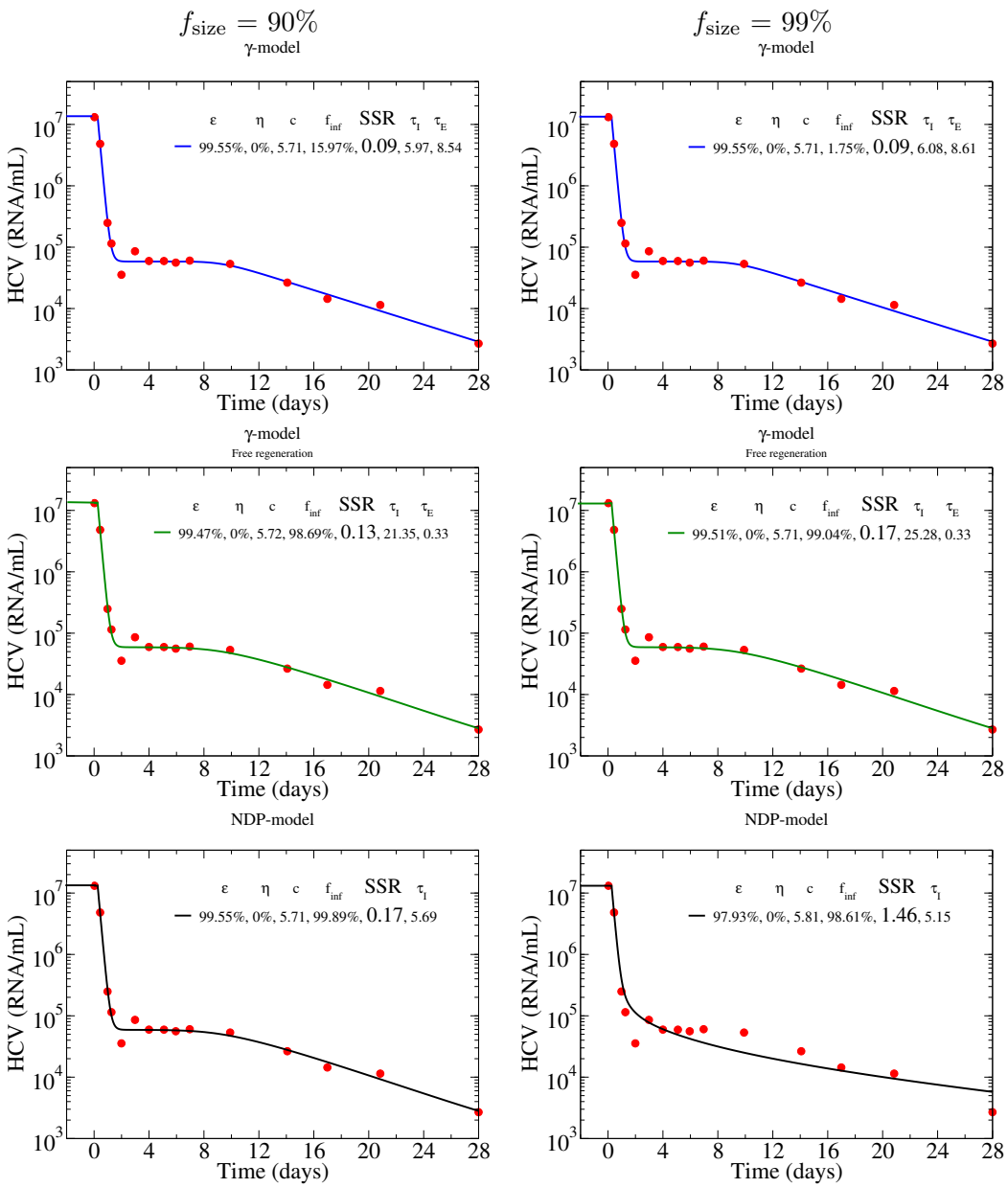

Figure 7.8: **Fits to triphasic decay patient-T data from Reluga et al. (2009) treated with IFN.** The top rows show the γ-model fit to the patient data with the regeneration rate parameters either constrained (blue lines) or free (green lines). The bottom row is the NDP model (Black lines) fit. In the left column it is assumed that the infected liver size is 90% of its original size, and in the right column $f_{\text{size}} = 99\%$. The steady state viral load is $\bar{V} = 1.31 \times 10^7$ HCV$\frac{\text{RNA}}{\text{mL}}$ and the delay time is $t_0 = 0.26$ d. Other parameter values are shown in Table A.7.

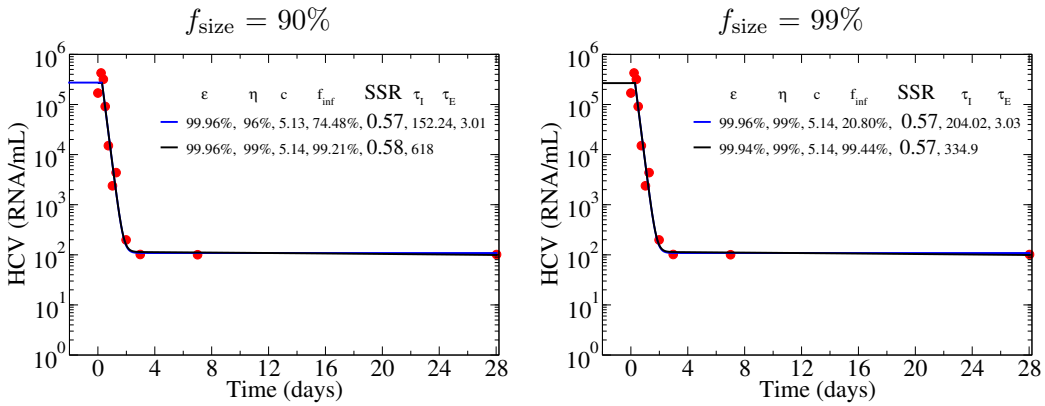

Figure 7.9: **Fits to flat partial decay patient-24 data from Dixit et al. (2004) treated with IFN+RBV.** The γ-model (black lines) and NDP model (blue lines) fits to patient data are shown here. In the left column it is assumed that the infected liver size is 90% of its original size, and in the right column $f_{\text{size}} = 99\%$. The steady state viral load is $\bar{V} = 2.6 \times 10^5$ HCV$\frac{\text{RNA}}{\text{mL}}$ and the delay time is $t_0 = 0.29$ d. Other parameter values are shown in Table A.8.

in Figure 7.9. Both models do equally well in fitting flat partial patient data, and predict a similar drug efficacy and clearance rate, though the γ-model does so with a smaller fraction of cells infected (i.e., smaller τ_I).

Chapter 8

Conclusion

Hepatitis C is a serious infectious disease of the liver. About 150 million people are chronically infected with the HCV, and more than 350,000 people die every year from hepatitis C-related liver diseases [76]. While experimental studies have been limited, the analysis of viral decay under treatment, with the help of mathematical models, has provided the most useful information. Mathematical models have allowed for the evaluation of the antiviral efficacy and estimation of important parameters. However, current mathematical models of HCV kinetics, based on a set of ordinary differential equations (ODEs), neglect any delay between the moment of cell infection and the release of new virions, and also assume that the infectious cell lifespan is exponentially distributed over time, meaning that every cell has an equal probability of dying at any time. Moreover, these models have not implemented much of the available independent biological information on HCV dynamics and the HCV-infected liver.

In this thesis, we have reviewed the state of HCV kinetic modelling and introduced a new model with an eclipse phase and flexible delay distributions to represent both the eclipse phase and infectious cell lifespan. Our new γ-model, is a multi-stage, ODE model which imposes a gamma-distributed eclipse phase to account for known delays between infection and virus release, and is able to consider both exponential and gamma-

distributed infectious cell lifespans, enabling it to capture the dynamics of most reasonable processes by which infectious cells may be lost, except infectious cell cure (see below).

We determined that the addition of an eclipse phase, be it exponential or gamma-distributed, does not affect the first phase decay following administration of IFN therapy. Like previous ODE models, the first phase decay in the γ-model depends only on antiviral efficacy at blocking virus production, ε, and on the viral clearance rate, c. As such, our model's estimate of the efficacy of IFN therapy, which relies primarily on fitting this first phase decay, agrees with that of previous ODE models which did not include an eclipse phase. This was an important confirmation that previous results have not been adversely affected by the neglect of the eclipse phase. Interestingly, we found that long, gamma-distributed eclipse phases will yield a shoulder, right after the first phase decay, whose length increases as the eclipse phase length increases. This is not the case when the eclipse phase duration is exponentially distributed. In our model, cells in the eclipse phase are infected but are not yet producing virus. One possible extension of this model would be to consider these cells as still susceptible to co-infection. For example, the co-infection of an eclipse cell by a defective interfering particle could have important implications for HCV VK [42, 60].

We also found that implementing the infectious cell lifespan using a gamma-distribution rather than an exponential leads to a more abrupt and more "wavy" VK decay. Since both distributions for the infectious cell lifespan represent different biological processes, more frequently sampled data over longer periods of time after the first phase decay would provide a clearer picture of the shape and rate of that last phase decay. This, in turn, might make it possible to determine which process for the loss of infectious cells dominates. Unfortunately, such data is not currently available. It is also important to note that our new model presented here does not explicitly model the spontaneous curing of infectious cells. This would be a valuable extension to our model, well-worth

investigating in future work, as spontaneous curing of infectious cells might also affect the VK decay in the last phase.

We then went on to compare the traditional ODE model for HCV developed by Neumann, Dahari and Perelson (NDP) to our new model. In fitting both models against experimental data, we constrained certain parameters using known, measured quantities about HCV-infected liver, such as liver size, number of hepatocytes in the liver, and the fraction of liver infected. In the γ-model, we assumed the action of the antivirals were the same as those adopted in the NDP model (IFN down regulates viral production while RBV decreases HCV infectivity). Importantly, we found that the addition of an eclipse phase (of duration that is either exponential or gamma-distributed), and the use of either an exponential or gamma-distributed infectious cell lifespan had no effect on estimates of IFN antiviral efficacy (i.e., of any antiviral acting on viral production). Our analysis also yielded that efficacy of antivirals acting on infection rate (e.g., RBV) cannot reliably be determined by either models from patient VK alone.

We analyzed the results of the γ and NDP model to investigate their ability to reproduce and explain the three different VK profiles observed experimentally in HCV patients under antiviral treatment: biphasic, triphasic and flat partial decays. Both models were able to accomplish all observed VK profiles in patients under the same conditions.

In both models, biphasic decay was explained by shorter lived infected cells which suggests a smaller fraction of the liver infected. Most studies on the fraction of hepatocytes infected in chronically HCV-infected patients report a relatively small fraction of liver infected, which is consistent with our model-predicted f_{infec} values for biphasic decays, the most common VK pattern observed in patients.

There were two ways of explaining triphasic VK, one only available in the new γ-model. One way, which was adopted from current mathematical models, is to assume that a large fraction of liver is infected, i.e., $f_{\text{infec}} \sim 99\%$. The number of infected cells is

then several orders of magnitude larger than the number of uninfected cells. In this case, a large regeneration rate of uninfected and infected hepatocytes r_T and r_I is required. We have shown, however, in Chapter 3 that livers generally have similar capacity of regeneration do not vary much from patient to patient. Therefore we considered an alternative option for producing the triphasic decline: a long eclipse phase in the γ-model which yields a VK shoulder which lasts longer as the length of the eclipse phase increases. The reported values for τ_E in vitro vary from a few hours to several days [79]. A long eclipse phase duration in vivo could perhaps be due to the induction of an antiviral defense pathway by HCV [79] which could delay viral replication (i.e., lengthen the eclipse phase).

Flat decay requires the infectious cell lifespan to be quite large, enabling the HCV titer to settle into a new lower level and remains constant (to make the VK flat) which, in turn, given our constraints, implies that a large fraction of the liver is infected. Thus, both models suggest a possible cause for the flat response seen in a limited number of patients: these patients would have a much larger fraction of their liver infected than those which exhibit biphasic or triphasic viral decay under therapy due to long-lived infectious cells, possibly owing to a poor immune response against HCV. But is there really such a thing as a flat partial response? Closer inspection reveals that flat VK responses are only ever observed when VK data is collected up to 28 days. Interestingly, data exhibiting a triphasic decay contains a flat shoulder which can sometimes last up to 28 days. This suggests that if data had been collected for longer in patients exhibiting a flat VK response, a third decay phase indicative of triphasic decay might have been observed.

The γ-model with gamma-distributed lifespans produced same VK with similar dynamics as other exponentially distributed models (plus reproducing triphasic VK, while incorporating long gamma-distributed eclipse phase), but it can help establish more realistic parameters by imposing biological constraints.

The model discussed here, while providing valuable insight into the dynamics of HCV infection and treatment, is a starting point for further extensions. For example, a gamma-distributed model which incorporates drug resistance would be required to capture therapy with current, standard therapy with direct acting antivirals.

Appendix A

Parameter values

Parameter	Units	Top-left	Top-right	Bottom-left	Bottom-right
r_T	d^{-1}	0.12	0.12	0.45	10
r_E	d^{-1}	0.12	0.12	0	0
r_I	d^{-1}	0.05	0.05	0.45	9.99
p	$\frac{\mathrm{RNA}}{\mathrm{mL}\cdot\mathrm{d}\cdot\mathrm{cell}}$	2.05×10^{-3}	1.52×10^{-2}	1.05×10^{-3}	5.99×10^{-4}
β	$\frac{\mathrm{mL}}{\mathrm{RNA}\cdot\mathrm{d}}$	1.56×10^{-9}	1.56×10^{-10}	6.51×10^{-9}	1.29×10^{-8}
s	$\mathrm{cell}\cdot\mathrm{d}^{-1}$	0	0	7.11×10^{4}	6.67
$1/\tau_T$	d^{-1}	0	0	2.90×10^{-2}	7.86×10^{-5}

Table A.1: **Estimated parameters for patient-15.** The first and second columns give the parameter values for fitting the γ-model to data at $f_{\text{size}} = 90\%$ and 99%, respectively, and the fourth and fifth columns give the parameter values for fitting the NDP model to data at $f_{\text{size}} = 90\%$ and 99%, respectively, in Figure 7.2.

Parameter	Units	Top-left	Top-right	Bottom-left	Bottom-right
r_T	d^{-1}	0.12	0.12	1.24	2.94
r_E	d^{-1}	0.12	0.12	0	0
r_I	d^{-1}	0.05	0.05	1.24	2.94
p	$\frac{\mathrm{RNA}}{\mathrm{mL}\cdot\mathrm{d}\cdot\mathrm{cell}}$	2.26×10^{-2}	1.84×10^{-1}	5.80×10^{-3}	1.77×10^{-2}
β	$\frac{\mathrm{mL}}{\mathrm{RNA}\cdot\mathrm{d}}$	3.03×10^{-10}	3.03×10^{-11}	5.52×10^{-9}	1.48×10^{-9}
s	$\mathrm{cell}\cdot\mathrm{d}^{-1}$	0	0	1	1.36×10^{3}
$1/\tau_T$	d^{-1}	0	0	1×10^{-7}	1×10^{-7}

Table A.2: **Estimated parameters for patient-16.** The first and second columns give the parameter values for fitting the γ-model to data at $f_{\text{size}} = 90\%$ and 99%, respectively, and the fourth and fifth columns give the parameter values for fitting the NDP model to data at $f_{\text{size}} = 90\%$ and 99%, respectively, in Figure 7.3.

Parameter	Units	Top-left	Top-right	Bottom-left	Bottom-right
r_T	d^{-1}	0.12	0.12	0.19	9.84
r_E	d^{-1}	0.12	0.12	0	0
r_I	d^{-1}	0.05	0.05	0.001	1.51
p	$\frac{\mathrm{RNA}}{\mathrm{mL}\cdot\mathrm{d}\cdot\mathrm{cell}}$	7.36×10^{-3}	5.89×10^{-2}	2.63×10^{-2}	1.04×10^{-1}
β	$\frac{\mathrm{mL}}{\mathrm{RNA}\cdot\mathrm{d}}$	1.75×10^{-9}	1.75×10^{-10}	1.81×10^{-9}	4.10×10^{-10}
s	$\mathrm{cell}\cdot\mathrm{d}^{-1}$	0	0	1	4.20×10^{5}
$1/\tau_T$	d^{-1}	0	0	9.06×10^{-3}	1.93×10^{-1}

Table A.3: **Estimated parameters for patient-23.** The first and second columns give the parameter values for fitting the γ-model to data at $f_{\text{size}} = 90\%$ and 99%, respectively, and the fourth and fifth columns give the parameter values for fitting the NDP model to data at $f_{\text{size}} = 90\%$ and 99%, respectively, in Figure 7.4

Parameter	Units	Top-left	Top-right	Bottom-left	Bottom-right
r_T	d^{-1}	0.12	0.12	0.11	0.02
r_E	d^{-1}	0.12	0.12	0	0
r_I	d^{-1}	0.05	0.05	0.11	0.02
p	$\frac{\mathrm{RNA}}{\mathrm{mL}\cdot\mathrm{d}\cdot\mathrm{cell}}$	1.99×10^{-4}	1.48×10^{-3}	5.71×10^{-4}	5.07×10^{-3}
β	$\frac{\mathrm{mL}}{\mathrm{RNA}\cdot\mathrm{d}}$	3.29×10^{-8}	3.29×10^{-9}	5.33×10^{-8}	4.58×10^{-9}
s	$\mathrm{cell}\cdot\mathrm{d}^{-1}$	0	0	1	1.09×10^{3}
$1/\tau_T$	d^{-1}	0	0	1.36×10^{-7}	1×10^{-7}

Table A.4: **Estimated parameters for patient-p31.** The first and second columns give the parameter values for fitting the γ-model to data at $f_{\mathrm{size}} = 90\%$ and 99%, respectively, and the fourth and fifth columns give the parameter values for fitting the NDP model to data at $f_{\mathrm{size}} = 90\%$ and 99%, respectively, in Figure 7.5.

Parameter	Units	Top-left	Top-right	Bottom-left	Bottom-right
r_T	d^{-1}	0.12	0.12	10	9.99
r_E	d^{-1}	0.12	0.12	0	0
r_I	d^{-1}	0.05	0.05	0.82	0.05
p	$\frac{\mathrm{RNA}}{\mathrm{mL}\cdot\mathrm{d}\cdot\mathrm{cell}}$	5.59×10^{-4}	4.73×10^{-3}	4.66×10^{-5}	7.77×10^{-5}
β	$\frac{\mathrm{mL}}{\mathrm{RNA}\cdot\mathrm{d}}$	2.37×10^{-8}	2.37×10^{-9}	2.01×10^{-6}	2.22×10^{-7}
s	$\mathrm{cell}\cdot\mathrm{d}^{-1}$	0	0	6.48×10^{7}	1
$1/\tau_T$	d^{-1}	0	0	1.47×10^{-3}	1.2×10^{-5}

Table A.5: **Estimated parameters for patient-34.** The first and second columns give the parameter values for fitting the γ-model to data at $f_{\mathrm{size}} = 90\%$ and 99%, respectively, and the fourth and fifth columns give the parameter values for fitting the NDP model to data at $f_{\mathrm{size}} = 90\%$ and 99%, respectively, in Figure 7.6.

Parameter	Units	Top-left	Top-right	Middle-left	Middle-right	Bottom-left	Bottom-right
r_T	d^{-1}	0.12	0.12	0.58	4.96	2.31	10
r_E	d^{-1}	0.12	0.12	0.58	4.96	0	0
r_I	d^{-1}	0.05	0.05	2.66	20.28	2.14	10
p	$\frac{\mathrm{RNA}}{\mathrm{mL}\cdot\mathrm{d}\cdot\mathrm{cell}}$	5.38×10^{-4}	9.90×10^{-4}	5.55×10^{-5}	4.99×10^{-5}	6.14×10^{-5}	6.58×10^{-5}
β	$\frac{\mathrm{mL}}{\mathrm{RNA}\cdot\mathrm{d}}$	7.88×10^{-9}	7.88×10^{-10}	3.81×10^{-8}	3.26×10^{-8}	1.52×10^{-7}	8.46×10^{-8}
s	$\mathrm{cell}\cdot\mathrm{d}^{-1}$	0	0	0	0	2.33	3.76×10^{8}
$1/\tau_T$	d^{-1}	0	0	0	0	1.04×10^{-7}	1.14×10^{-27}

Table A.6: **Estimated parameters for patient-2B.** The first and second columns give the parameter values for fitting the γ-model to data at $f_{\text{size}} = 90\%$ and 99%, respectively, with fixed regeneration rates. The third and fourth columns give the parameter values for fitting the γ-model to data at $f_{\text{size}} = 90\%$ and 99%, respectively, with free regeneration rates. The fifth and sixth columns the parameter values for fitting the NDP model to data at $f_{\text{size}} = 90\%$ and 99%, respectively, in Figure 7.7

Parameter	Units	Top-left	Top-right	Middle-left	Middle-right	Bottom-left	Bottom-right
r_T	d^{-1}	0.12	0.12	18.74	20.4	6.76	10
r_E	d^{-1}	0.12	0.12	18.74	20.4	0	0
r_I	d^{-1}	0.05	0.05	0.015	12.4	1.74	5.01
p	$\frac{\text{RNA}}{\text{mL}\cdot\text{d}\cdot\text{cell}}$	1.21×10^{-3}	1.04×10^{-1}	8.56×10^{-4}	7.74×10^{-4}	8.35×10^{-4}	7.82×10^{-4}
β	$\frac{\text{RNA}}{\text{mL}}$	9.12×10^{-10}	9.12×10^{-11}	1.42×10^{-7}	1.55×10^{-7}	5.14×10^{-8}	1.052×10^{-6}
s	$\frac{\text{RNA}}{\text{cell}\cdot\text{d}}$	0	0	0	0	1.06	1×10^{3}
$1/\tau_T$	d^{-1}	0	0	0	0	3.53×10^{-12}	9.36×10^{-3}

Table A.7: **Estimated parameters for patient-T.** The first and second columns give the parameter values for fitting the γ-model to data at $f_{\text{size}} = 90\%$ and 99%, respectively, with fixed regeneration rates. The third and fourth columns give the parameter values for fitting the γ-model to data at $f_{\text{size}} = 90\%$ and 99%, respectively, with free regeneration rates. The fifth and sixth columns the parameter values for fitting the NDP model to data at $f_{\text{size}} = 90\%$ and 99%, respectively, in Figure 7.8

Parameter	Units	Top-left	Top-right	Bottom-left	Bottom-right
r_T	d^{-1}	0.12	0.12	6.99	2.96
r_E	d^{-1}	0.12	0.12	0	0
r_I	d^{-1}	0.05	0.05	6.95	10
p	$\frac{\mathrm{RNA}}{\mathrm{mL}\cdot\mathrm{d}\cdot\mathrm{cell}}$	2.08×10^{-5}	6.79×10^{-5}	1.54×10^{-5}	1.40×10^{-5}
β	$\frac{\mathrm{mL}}{\mathrm{RNA}\cdot\mathrm{d}}$	4.47×10^{-8}	4.47×10^{-9}	2.66×10^{-9}	1.32×10^{-4}
s	$\mathrm{cell}\cdot\mathrm{d}^{-1}$	0	0	1.03×10^{4}	1.96×10^{10}
$1/\tau_T$	d^{-1}	0	0	0.1	0.01

Table A.8: **Estimated parameters for patient-24.** The first and second columns give the parameter values for fitting the γ-model to data at $f_{\mathrm{size}} = 90\%$ and 99%, respectively, and the fourth and fifth columns give the parameter values for fitting the NDP model to data at $f_{\mathrm{size}} = 90\%$ and 99%, respectively, in Figure 7.9

Bibliography

[1] V. Agnello, G. Abel, G. B. Knight, and E. Muchmore. Detection of widespread hepatocyte infection in chronic hepatitis C. *Hepatology*, 28(2):573–584, August 1998.

[2] H. J. Alter. HCV natural history: The retrospective and prospective in perspective. *Hepatology*, 43(4):550–552, Oct 2005.

[3] H. Bantel and K. S. Osthoff. Apoptosis in hepatitis C virus infection. *Cell death and differentiation*, 10(1):s48–s58, Jan 2003.

[4] R. Bartenschlager, F. L. Cosset, and V. Lohmann. Hepatitis C virus replication cycle. *Hepatology*, 53:583–585, April 2010.

[5] F. C. Bekkering, A. U. Neumann, J. T. Brouwer, R. S. L. Drummer, and S. W. Schalm. Changes in antiviral effectiveness of interferon after dose reduction in chronic hepatitis C patients: a case control studys. *BioMed Central Gastroenterology*, 1(14), Dec 2001.

[6] T. Berg, M. von Wagner, S. Nasser, C. Sarrazin, T. Heintges, T. Gerlach, P. Buggisch, T. Goeser, J. Rasenack, G. R. Pape, W. E. Schmidt, B. Kallinowski, H. Klinker, U. Spengler, P. Martus, U. Alshuth, and S. Zeuzem. Extended treatment duration for hepatitis C virus type 1: comparing 48 versus 72 weeks of peginterferon-alfa-2a plus ribavirin. *Gastroenterology*, 130(4):1086–1097, April 2006.

[7] K. D. Bissig, S. F. Wieland, P. Tran, M. Isogawa, T. T. Le, F. V. Chisari, and I. M. Verma. A critical role for the chimpanzee model in the study of hepatitis C. *Clinical Investigation*, 120(3):924–930, March 2010.

[8] K. J. Blight, J. A. McKeating, and C. M. Rice. Highly permissive cell lines for subgenomic and genomic hepatitis C virus RNA replication. *Virology*, 76(24):13001–13014, Dec 2002.

[9] J. Bukh. A critical role for the chimpanzee model in the study of hepatitis C. *Hepatology*, 39(6):1469–1475, May 2004.

[10] F. Calabrese, P. Pontisso, E. Pettenazzo, L. Benvegn, A. Vario, L. Chemello, A. Alberti, and M. Valente. Liver cell apoptosis in chronic hepatitis C correlates with histological but not biochemical activity or serum HCV-RNA levels. *Hepatology*, 31(5):1153–1159, May 2000.

[11] K. M. Chang, R. Thimme, J. J. Melpolder, D. Oldach, J. Pemberton, J. M. Loudis, J. G. McHutchison, H. J. Alter, and F. V. Chisari. Differential CD4+ and CD8+ T-cell responsiveness in hepatitis C virus infection. *Hepatology*, 33(1):267–276, January 2001.

[12] M. Cherian and Y. Kang. Metallothionein and liver cell regeneration. *Experimental biology and medicine*, 231(2):138–144, Feb 2006.

[13] C. H. Chou, H. F. Tsai, Y. Y. Wu, C. Y. Hu, L. H. Hwang, P. I. Hsu, and P. N. Hsu. Hepatitis C virus core protein modulates TRAIL-mediated apoptosis by enhancing bid cleavage and activation of mitochondria apoptosis signaling pathway. *Immunology*, 174(4):2160–2166, February 2005.

[14] G. Colloredo, M. Guido, A. Sonzogni, and G. Leandro. Impact of liver biopsy size on histological evaluation of chronic viral hepatitis: The smaller the sample, the milder the disease. *Hepatology*, 39(2):239–244, August 2003.

[15] P. Colombatto, L. Civitano, F. Oliveri, B. Coco, P. Ciccorossi, D. Flichman, M. Campa, F. Bonino, and M. R. Brunetto. Sustained response to interferon-ribavirin combination therapy predicted by a model of hepatitis C virus dynamics using both HCV RNA and alanine aminotransferase. *Antiviral Therapy*, 8(6):519–530, Dec 2003.

[16] H. Dahari, J. E. L. Almer, E. Kallwitz, R. M. Riberio, S. J. Cotler, T. J. Layden, and A. S. Perelson. A mathematical model of hepatitis C virus dynamics in patients with high baseline viral loads or advanced liver disease. *Gastroenterology*, 136(4):1402–1409, April 2009.

[17] H. Dahari, B. S. Jr, A. S. Perelson, and S. L. Uprichard. Modeling subgenomic hepatitis C virus RNA kinetics during treatment with alpha interferon. *Virology*, 83(13):6383–6390, July 2009.

[18] H. Dahari, A. Lo, R. M. Riberio, and A. S. Perelson. Modeling hepatitis C virus dynamics: Liver regeneration and critical drug efficacy. *Theoretical Biology*, 247(2):371–381, July 2007.

[19] H. Dahari, M. Major, X. Zhang, K. Mihalik, C. Rice, A. Perelson, S. Feinstone, and A. Neumann. Mathematical modeling of primary hepatitis C infection: Noncytolytic clearance and early blockage of virion production. *Gastroenterology*, 128(4):1056–1066, April 2005.

[20] H. Dahari, M. Major, X. Zhang, K. Mihalik, C. Rice, A. Perelson, S. Feinstone, and A. Neumann. Second hepatitis C replication compartment indicated by viral dynamics during liver transplantation. *Hepatology*, 42(4):491–498, April 2005.

[21] H. Dahari, R. M. Ribeiro, C. M. Rice, and A. S. Perelson. Mathematical modeling of subgenomic hepatitis C virus replication in Huh-7 cells. *Virology*, 81(2):750–760, January 2007.

[22] H. Dahari, R. M. Riberio, and A. S. Perelson. Triphasic decline of hepatitis C virus RNA during antiviral therapy. *Hepatology*, 46(1):16–21, July 2007.

[23] H. Dahari, E. Shudo, S. J. Cotler, T. J. Layden, , and A. S. Perelson. Modeling hepatitis C virus kinetics: the relationship between the infected cell loss rate and the final slope of viral decay. *Antiviral Therapy*, 14(3):459–464, 2009.

[24] S. de Lucas, J. Bartolome, E. RodrguezInigo, M. Casqueiro, A. Millan, M. Ruiz-Moreno, H. Oliva, and V. Carreno. Distribution of hepatitis C virus infection in liver biopsies from children and adults with chronic hepatitis C. *Medical Virology*, 64(1):1–5, May 2001.

[25] L. Deng, T. Adachi, K. Kitayama, Y. Bungyoku, S. Kitazawa, S. Ishido, I. Shoji, and H. Hotta. Hepatitis C virus infection induces apoptosis through a bax-triggered, mitochondrion-mediated, caspase 3-dependent pathway. *Virology*, 82(21):10375–10385, Nov 2008.

[26] N. M. Dixit, J. E. L. Almer, T. J. Layden, and A. S. Perelson. Modelling how ribavirin improves interferon response rates in hepatitis C virus infection. *Nature*, 432(7019):922–924, Dec 2004.

[27] N. Fausto. Liver regeneration and repair: Hepatocytes, progenitor cells, and stem cells. *Hepatology*, 39(6):1477–1487, June 2004.

[28] T. Fukumoto, T. Berg, Y. Ku, W. O. Bechstein, M. Knoop, H. Lemmens, H. Lobeck, U. Hopf, and P. Neuhaus. Viral dynamics of hepatitis C early after orthotopic liver transplantation: Evidence for rapid turnover of serum virions. *Hepatology*, 24(6):1351–1354, December 1996.

[29] J. Gottwein, T. Scheel, T. Jensen, J. Lademann, J. Prentoe, M. Knudsen, A. Hoegh, and J. Bukh. Development and characterization of hepatitis C virus genotype 1-7

cell culture systems: role of CD81 and scavenger receptor class B type I and effect of antiviral drugs. *Hepatology*, 49(2):364–370, Feb 2009.

[30] J. Guo, R. Yan, G. Xu, and W. Li. Construction of the vero cell culture system that can produce infectious HCV particles. *Molecular Biology Reports*, 36(1):111–120, Jan 2009.

[31] E. Herrmann, J. H. Lee, G. Marinos, M. Modi, and S. Zeuzem. Effect of ribavirin on hepatitis C viral kinetics in patients treated with pegylated interferon. *Hepatology*, 37(6):1351–1358, June 2003.

[32] C. Hzode, N. Forestier, G. Dusheiko, P. Ferenci, S. Pol, T. Goeser, J. P. Bronowicki, M. B. S. Gharakhanian, L. Bengtsson, L. McNair, S. George, T. Kieffer, A. Kwong, R. S. Kauffman, J. Alam, J. M. Pawlotsky, and S. Zeuzem. An in vitro model of hepatitis C virion production. *New England Journal of Medicine*, 360:1839–1850, April 2009.

[33] J. Jo, V. Lohmann, R. Bartenschlager, and R. Thimme. Experimental models to study the immunobiology of hepatitis C virus. *General Virology*, 92:477–493, 2011.

[34] R. P. Kannan, L. L. Hensley, L. E. Evers, S. M. Lemon, , and D. R. McGivern. Hepatitis C virus infection causes cell cycle arrest at the level of initiation of mitosis. *Virology*, 85(16):7989–8001, August 2011.

[35] S. K. Leea, S. O. Parka, C. O. Joeb, and Y. S. Kim. Interaction of HCV core protein with 14-3-3ϵ protein releases bax to activate apoptosis. *Biochemical and biophysical research communications*, 352(3):756–762, January 2007.

[36] B. D. Lindenbach, M. J. Evans, A. J. Syder, B. Wlk, T. L. Tellinghuisen, C. C. Liu, T. Maruyama, R. O. Hynes, D. R. Burton, J. A. McKeating, and C. M. Rice. Complete replication of hepatitis C virus in cell culture. *Science*, 309(5734):623–626, July 2005.

[37] B. D. Lindenbach and C. M. Rice. Unravelling hepatitis C virus replication from genome to function. *Nature*, 436(18):933–938, August 2005.

[38] A. L. Lloyd. The dependence of viral parameter estimates on the assumed viral life cycle: limitations of studies of viral load data. *Proc. R. Soc. Lond. B*, 268(1469):847–854, April 2001.

[39] A. L. Lloyd. Destabilization of epidemic models with the inclusion of realistic distributions of infectious periods. *Proc. R. Soc. Lond. B*, 268(1470):985–993, May 2001.

[40] R. Loomba, M. Rivera, R. McBurney, Y. Park, V. H. Williams, B. Rehermann, H. Alter, S. Herrine, T. Liang, J. Hoofnagle, and T. Heller. The natural history of acute hepatitis C: Clinical presentation, laboratory findings and treatment outcomes. *Alimentary Pharmacology and Therapeutics*, 33(5):559–565, Mar 2011.

[41] C. A. Lzaro, M. Chang, W. Tang, J. Campbell, D. G. Sullivan, D. R. Gretch, L. Corey, R. W. Coombs, , and N. Fausto. Hepatitis C virus replication in transfected and serum-infected cultured human fetal hepatocytes. *The American Journal of Pathology*, 170(2):478–489, February 2007.

[42] M. Martell, J. I. Esteban, J. Quer, J. Genesc, A. Weiner, R. Esteban, J. Guardia, and J. Gmez. Hepatitis C virus (HCV) circulates as a population of different but closely related genomes: quasispecies nature of HCV genome distribution. *Virology*, 66(5):3225–3229, May 1992.

[43] J. H. Mathews and K. D.Fink. *Fitting Models to Biological Data Using Linear and Nonlinear Regression: A Practical Guide to Curve Fitting.* GraphPad Software Inc, San Diego, CA, 2003.

[44] J. G. McHutchison, G. T. Everson, S. C. Gordon, I. M. Jacobson, M. Sulkowski, R. Kauffman, L. McNair, J. Alam, and A. J. Muir. Telaprevir with peginterferon and

ribavirin for chronic HCV genotype 1 infection. *New England Journal of Medicine*, 360:1827–1838, April 2009.

[45] R. G. Meeks, S. D. Harrison, and R. J. Bull. *Hepatotoxicology*. CRC press, Boca Raton, Florida, 1991.

[46] G. K. Michalopoulos and M. C. DeFrances. Liver regeneration. *Science*, 276(5309):60–66, April 1997.

[47] N. Nagasue, H. Yukaya, Y. Ogawa, H. Kohno, and T. Nakamura. Human liver regeneration after major hepatic resection. a study of normal liver and livers with chronic hepatitis and cirrhosis. *Annals of Surgery*, 206(1):30–39, 1987.

[48] J. A. Nelder and R. Mead. A simplex method for function minimization. *The Computer Journal*, 7(4):308–313, 1965.

[49] A. U. Neumann, N. P. Lam, H. Dahari, D. R. Gretch, T. E. Wiley, T. J. Layden, and A. S. Perelson. Hepatitis C viral dynamics in vivo and the antiviral efficacy of interferon-α therapy. *Science*, 282(5386):103–107, 2 October 1998.

[50] T. Nguyen, A. SedghiVaziriand, L. Wilkes, T. Mondala, P. Pockros, K. Lindsay, and J. McHutchison. Fluctuations in viral load (HCV RNA) are relatively insignificant in untreated patients with chronic HCV infection. *Viral hepatitis*, 3(2):75–78, Mar 1996.

[51] M. A. Nowak, A. L. Lloyd, G. M. V. andT A Wiltrout, L. M. Wahl, N. Bischofberger, J. Williams, A. Kinter, A. S. Fauci, V. M. Hirsch, and J. D. Lifson. Viral dynamics of primary viremia and antiretroviral therapy in simian immunodeficiency virus infection. *Virology*, 71(10):7518–7525, October 1997.

[52] H. Nuriya, K. Inoue, T. Tanaka, Y. Hayashi, T. Hishima, N. Funata, K. Kaji, S. Hayashi, S. Kaneko, and M. Kohara. Detection of hepatitis B and C viruses

in almost all hepatocytes by modified pcr-based in situ hybridization. *Clinical Microbiology*, 48(11):3843–3851, Nov 2010.

[53] N. Pal, C. Jin, and W. K. Lim. *Handbook of Exponential and Related Distributions for Engineers and Scientists*. Chapman and Hall/CRC, Boca Raton, Florida, 2006.

[54] R. Pei, H. Chen, L. Lu, W. Zhu, S. Beckebaum, V. Cicinnati, M. Lu, and X. Chen. Hepatitis C virus infection induces the expression of amphiregulin, a factor related to the activation of cellular survival pathways and required for efficient viral assembly. *Virology*, 92(10):2237–2248, Oct 2011.

[55] A. S. Perelson, P. Essunger, Y. Cao, M. Vesanen, A. Hurley, K. Saksela, M. Markowitz, and D. D. Ho. Decay characteristics of HIV-1-infected compartments during combination therapy. *Nature*, 387(6629):188–191, May 1997.

[56] A. S. Perelson, E. Herrmann, F. Micol, and S. Zeuzem. New kinetic models for the hepatitis C virus. *Hepatology*, 42(4):749–754, Oct 2005.

[57] A. S. Perelson and P. W. Nelson. Mathematical analysis of HIV-I: Dynamics in vivo. *Society for Industrial and Applied Mathematics*, 41(1):3–44, March 1999.

[58] A. S. Perelson, A. U. Neumann, M. Markowitz, J. M. Leonard, and D. D. Ho. HIV-1 dynamics in vivo: Virion clearance rate, infected cell life-span, and viral generation time. *Science*, 271(5255):1582–1586, March 1996.

[59] F. Poordad, J. McCone, B. R. Bacon, S. Bruno, M. P. Manns, M. S. Sulkowski, I. M. Jacobson, K. R. Reddy, Z. D. Goodman, N. Boparai, M. J. DiNubile, V. Sniukiene, C. A. Brass, J. K. Albrecht, and J. P. Bronowicki. Boceprevir for untreated chronic HCV genotype 1 infection. *New England Journal of Medicine*, 364:1195–11206, March 2011.

[60] A. M. Prince, T. H. Byron, T. S. Parker, and D. M. Levine. Visualization of hepatitis C virions and putative defective interfering particles isolated from low-density lipoproteins. *Viral Hepatitis*, 3(1):11–17, January 1996.

[61] T. C. Reluga, H. Dahari, and A. S. Perelson. Analysis of hepatitis C virus infection models with hepatocyte homeostasis. *SIAM Journal on applied mathematics*, 69(4):999–1023, January 2009.

[62] M. G. Retortillo, X. Forns, A. Feliu, E. Moitinho, J. Costa, M. Navasa, A. Rimola, and J. Rodes. Hepatitis C virus kinetics during and immediately after liver transplantation. *Hepatology*, 35(3):680–687, March 2002.

[63] R. M. Ribeiro, J. Layden-Almer, K. A. Powers, T. J. Layden, and A. S. Perelson. Dynamics of alanine aminotransferase during hepatitis C virus treatment. *Hepatology*, 38(2):509–517, August 2003.

[64] B. Robertson, G. Myers, C. Howard, T. Brettin, J. Bukh, B. Gaschen, T. Gojobori, G. Maertens, M. Mizokami, O. Nainan, S. Netesov, K. Nishioka, T. Shini, P. Simmonds, D. Smith, L. Stuyver, and A. Weiner. Classification, nomenclature, and database development for hepatitis C virus (HCV) and related viruses: proposals for standardization. *Archives of Virology*, 143(12):2493–2503, Dec 1998.

[65] E. RodrguezInigo, J. M. L. Alcorocho, J. Bartolome, N. OrtizMovilla, M. Pardo, and V. Carreno. Percentage of hepatitis C virus-infected hepatocytes is a better predictor of response than serum viremia levels. *Molecular Diagnostics*, 7(4):535–543, October 2005.

[66] C. W. Sheparda, L. Finelli, and M. J. Alterc. Global epidemiology of hepatitis C virus infection. *The Lancet infectious diseases*, 5(9):558–567, September 2005.

[67] M. A. Stafford, L. Corey, Y. Cao, E. S. Daar, D. D. Ho, and A. S. Perelson. Modeling plasma virus concentration during primary HIV infection. *Theoretical biology*, 203(3):285–301, April 2000.

[68] D. B. Strader and L. B. Seeff. A brief history of the treatment of viral hepatitis C. *Clinical Liver Disease*, 1(1), March 2012.

[69] Y. N. Takigawa, M. N. Fujii, L. Deng, S. Kitazawa, S. Ishido, K. Sada, and H. Hotta. Non-structural protein 4A of hepatitis C virus accumulates on mitochondria and renders the cells prone to undergoing mitochondria-mediated apoptosis. *Clinical Microbiology*, 87(7):1935–1945, July 2006.

[70] S. L. Tan. *Hepatitis C viruses: Genomes and molecular biology*. Horizon Bioscience, Norfolk, UK, 2006.

[71] V. TenCate, B. S. Jr, S. J. Cotler, and S. L. Uprichard. Potential treatment options and future research to increase hepatitis C virus treatment response rate. *Hepat Med.*, 2:125–145, February 2010.

[72] J. M. Timpe, Z. Stamataki, A. Jennings, K. Hu, M. J. Farquhar, H. J. Harris, A. Schwarz, I. Desombere, G. L. Roels, P. Balfe, and J. A. McKeating. Hepatitis C virus infection. *Clinical Microbiology and Infection*, 11(2):86–94, February 2005.

[73] J. M. Timpe, Z. Stamataki, A. Jennings, K. Hu, M. J. Farquhar, H. J. Harris, A. Schwarz, I. Desombere, G. L. Roels, P. Balfe, and J. A. McKeating. Hepatitis C virus cell-cell transmission in hepatoma cells in the presence of neutralizing antibodies. *Hepatology*, 47(1):17–24, January 2008.

[74] G. Vona, R. Tuveri, O. Delpuech, A. Vallet, D. Canioni, G. Ballardini, J. B. Trabut, B. L. Bail, B. Nalpas, F. Carnot, S. Pol, C. Brechot, and V. Thiers. Intrahepatic hepatitis C virus RNA quantification in microdissected hepatocytes. *Hepatology*, 40(4):682–688, April 2004.

[75] X. Wang, E. Montini, M. AlDhalimy, E. Lagasse, M. Finegold, and M. Grompe. Kinetics of liver repopulation after bone marrow transplantation. *American Journal of Pathology*, 16(12):565–574, August 2002.

[76] World Health Organization. http://www.who.int/mediacentre/factsheets/fs164/en. *Hepatitis C. Fact sheet No. 164*, revised July 2012.

[77] N. Yamanka, E. Okamoto, E. Kawamura, T. Kato, T. Oriyama, J. Fujimoto, K. Furukawa, T. Tanaka, F. Tomoda, and W. Tanaka. Dynamics of normal and injured human liver regeneration after hepatectomy as assessed on the basis of computed tomography and liver function. *Hepatology*, 18(1):79–85, Jul 1993.

[78] M. L. Yu, C. Y. Dai, J. F. Huang, C. F. Chiu, Y. H. C. Yang, N. J. Hou, L. P. Lee, M. Y. Hsieh, Z. Y. Lin, S. C. Chen, M. Y. Hsieh, L. Y. Wang, W. Y. Chang, and W. L. Chuang. Rapid virological response and treatment duration for chronic hepatitis c genotype 1 patients: A randomized trial. *Hepatology*, 47(6):1884–1893, may 2008.

[79] J. Zhong, P. Gastaminza, G. Cheng, S. Kapadia, T. Kato, D. R. Burton, S. F. Wieland, S. L. Uprichard, T. Wakita, and F. V. Chisari. Robust hepatitis C virus infection in vitro. *PNAS*, 102(26):9294–9299, June 2005.

Glossary

Abbreviations

DAAs Direct acting antivirals.

HCV Hepatitis C virus.

HIV Human immunodeficiency virus.

Huh-7 Human hepatoma cell line.

IFN Interferon.

JFH-1 Japanese fulminant hepatitis.

ODE Ordinary differential equation.

PCR Polymerase chain reaction.

RBV Ribavirin.

RNA Ribonucleic acid.

RT-PCR Reverse transcriptase polymerase chain reaction.

SSR Sum of squared residuals.

SVR Sustained virologic response.

VK Viral kinetic.

Variables and parameters

T Target cell (units: cells).

E Eclipse cell (units: cells).

I Infectious cell (units: cells).

D Dead/recovered cell (units: cells).

V Virus (units: HCV RNA $\cdot$ mL^{-1}).

$\bar{T}_{\mathbf{uninf}}$ Number of hepatocytes in an uninfected liver (units: cells).

$T_{\mathbf{max}}$ The maximum number of hepatocytes in a chronically infected liver (units: cells).

$f_{\mathbf{size}}$ Steady state size of the chronically HCV-infected liver expressed as a fraction of its size when uninfected.

$f_{\mathbf{infec}}$ Fraction of the hepatocytes of the chronically HCV-infected liver which are infected (E or I).

ε Antiviral efficacy on blocking virion production.

η Antiviral efficacy on reducing infection.

c Clearance rate of virions (units: d^{-1}).

β Rate of hepatocyte infection by virions (units: mL $\cdot$ RNA^{-1} $\cdot$ d^{-1}).

p Viral production rate (units: RNA $\cdot$ mL^{-1} $\cdot$ d^{-1} $\cdot$ cell^{-1}).

s Hepatocytes growth rate (units: cell $\cdot$ d^{-1}).

τ_T Average lifespan of uninfected, target hepatocytes (units: d).

τ_E Average duration of the eclipse phase (units: d).

τ_I Average lifespan of HCV-infected hepatocytes (units: d).

r_T Density-dependent regeneration rate of uninfected, target hepatocytes (units: d^{-1}).

r_E Density-dependent regeneration rate of infected hepatocytes in the eclipse phase (units: d^{-1}).

r_I Density-dependent regeneration rate of infectious hepatocytes (units: d^{-1}).

n_E Number of eclipse phase stages (shape parameter of the gamma distribution).

n_I Number of infectious phase stages (shape parameter of the gamma distribution).